

## Actin reorganization at the centrosomal area and the immune synapse regulates polarized secretory traffic of multivesicular bodies in T lymphocytes

Ana Bello-Gamboa , Marta Velasco , Solange Moreno , Gonzalo Herranz , Roxana Ilie , Silvia Huetos , Sergio Dávila , Alicia Sánchez , Jorge Bernardino De La Serna , Víctor Calvo & Manuel Izquierdo

To cite this article: Ana Bello-Gamboa , Marta Velasco , Solange Moreno , Gonzalo Herranz , Roxana Ilie , Silvia Huetos , Sergio Dávila , Alicia Sánchez , Jorge Bernardino De La Serna , Víctor Calvo & Manuel Izquierdo (2020) Actin reorganization at the centrosomal area and the immune synapse regulates polarized secretory traffic of multivesicular bodies in T lymphocytes, Journal of Extracellular Vesicles, 9:1, 1759926, DOI: [10.1080/20013078.2020.1759926](https://doi.org/10.1080/20013078.2020.1759926)

To link to this article: <https://doi.org/10.1080/20013078.2020.1759926>



© 2020 The Author(s). Published by Informa UK Limited, trading as Taylor & Francis Group on behalf of The International Society for Extracellular Vesicles.



[View supplementary material](#)



Published online: 19 Jun 2020.



[Submit your article to this journal](#)



Article views: 2593



[View related articles](#)



[View Crossmark data](#)



Citing articles: 3 [View citing articles](#)

RESEARCH ARTICLE



## Actin reorganization at the centrosomal area and the immune synapse regulates polarized secretory traffic of multivesicular bodies in T lymphocytes

Ana Bello-Gamboa<sup>a,b</sup>, Marta Velasco<sup>a,b</sup>, Solange Moreno<sup>a,b</sup>, Gonzalo Herranz<sup>a,b,c</sup>, Roxana Ilie<sup>a,b</sup>, Silvia Huetos<sup>a,b</sup>, Sergio Dávila<sup>a,b,d</sup>, Alicia Sánchez<sup>a,b,e</sup>, Jorge Bernardino De La Serna<sup>f,g</sup>, Víctor Calvo<sup>a,b</sup> and Manuel Izquierdo<sup>a,b</sup>

<sup>a</sup>Department of Metabolism and Cell Signaling, Instituto De Investigaciones Biomédicas Alberto Sols, CSIC-UAM, Madrid, Spain; <sup>b</sup>Departamento De Bioquímica, Facultad De Medicina, UAM Madrid, Spain; <sup>c</sup>Centro De Biología Molecular Severo Ochoa, Universidad Autónoma De Madrid, Cantoblanco, Madrid, Spain; <sup>d</sup>Nanostructured Functional Surfaces Program, IMDEA Nanociencia, Universidad Autónoma De Madrid, Cantoblanco, Madrid, Spain; <sup>e</sup>Neuroimmunology Unit, Puerta De Hierro-Segovia De Arana Health Research Institute, Madrid, Spain; <sup>f</sup>National Heart & Lung Institute, Faculty of Medicine, Imperial College London, South Kensington Campus, London, UK; <sup>g</sup>Central Laser Facility, Science and Technology Facilities Council, UK Research and Innovation. Research Complex at Harwell, Harwell-Oxford, UK

### ABSTRACT

T-cell receptor stimulation induces the convergence of multivesicular bodies towards the microtubule-organizing centre (MTOC) and the polarization of the MTOC to the immune synapse (IS). These events lead to exosome secretion at the IS. We describe here that upon IS formation centrosomal area F-actin decreased concomitantly with MTOC polarization to the IS. PKC $\delta$ -interfered T cell clones showed a sustained level of centrosomal area F-actin associated with defective MTOC polarization. We analysed the contribution of two actin cytoskeleton-regulatory proteins, FMNL1 and paxillin, to the regulation of cortical and centrosomal F-actin networks. FMNL1 $\beta$  phosphorylation and F-actin reorganization at the IS were inhibited in PKC $\delta$ -interfered clones. F-actin depletion at the central region of the IS, a requirement for MTOC polarization, was associated with FMNL1 $\beta$  phosphorylation at its C-terminal, autoregulatory region. Interfering all FMNL1 isoforms prevented MTOC polarization; nonetheless, FMNL1 $\beta$  re-expression restored MTOC polarization in a centrosomal area F-actin reorganization-independent manner. Moreover, PKC $\delta$ -interfered clones exhibited decreased paxillin phosphorylation at the MTOC, which suggests an alternative actin cytoskeleton regulatory pathway. Our results infer that PKC $\delta$  regulates MTOC polarization and secretory traffic leading to exosome secretion in a coordinated manner by means of two distinct pathways, one involving FMNL1 $\beta$  regulation and controlling F-actin reorganization at the IS, and the other, comprising paxillin phosphorylation potentially controlling centrosomal area F-actin reorganization.

**Abbreviations:** Ab, antibody; AICD, activation-induced cell death; AIP, average intensity projection; APC, antigen-presenting cell; BCR, B-cell receptor for antigen;  $C_m$ , centre of mass; cent2, centrin 2; cIS, central region of the immune synapse; CMAC, CellTracker™ Blue (7-amino-4-chloromethylcoumarin); cSMAC, central supramolecular activation cluster; CTL, cytotoxic T lymphocytes; DAG, diacylglycerol; DGK $\alpha$ , diacylglycerol kinase  $\alpha$ ; Dia1, Diaphanous-1; dSMAC, distal supramolecular activation cluster; ECL, enhanced chemiluminescence; ESCRT, endosomal sorting complex required for traffic; F-actin, filamentous actin; Fact-low cIS, F-actin-low region at the centre of the immune synapse; FasL, Fas ligand; FMNL1, formin-like 1; fps, frames per second; GFP, green fluorescent protein; HBSS, Hank's balanced salt solution; HRP, horseradish peroxidase; ILV, intraluminal vesicles; IS, immune synapse; MFI, mean fluorescence intensity; MHC, major histocompatibility complex; MIP, maximal intensity projection; MVB, multivesicular bodies; MTOC, microtubule-organizing centre; NS, not significant; PBL, peripheral blood lymphocytes; PKC, protein kinase C; PKC $\delta$ , protein kinase C  $\delta$  isoform; PLC, phospholipase C; PMA, phorbol myristate acetate; Pol. Index, polarization index; pSMAC, peripheral supramolecular activation cluster; PSF, point spread function; ROI, region of interest; SD, standard deviation; shRNA, short hairpin RNA; SEE, Staphylococcus enterotoxin E; SMAC, supramolecular activation cluster; TCR, T-cell receptor for antigen; T-helper (Th); TRANS, transmittance; WB, Western blot.

### ARTICLE HISTORY

Received 28 November 2019  
Revised 31 March 2020  
Accepted 13 April 2020



### KEYWORDS


T lymphocytes; immune synapse; actin cytoskeleton; protein kinase C  $\delta$ ; centrosome; multivesicular bodies; FMNL1; paxillin

### Introduction

T cell receptor (TCR) stimulation by antigen presented by major histocompatibility complex (MHC) molecules on an

antigen-presenting cell (APC) induces the formation of the immune synapse (IS), the convergence of secretory vesicles of T lymphocytes towards the microtubule-organizing centre (MTOC) and the polarization of the MTOC to the IS

**CONTACT** Manuel Izquierdo  [mizquierdo@iib.uam.es](mailto:mizquierdo@iib.uam.es)  Instituto De Investigaciones Biomédicas Alberto Sols, Lab C-20, CSIC-Universidad Autónoma De Madrid, Arturo Duperier 4 28029, Madrid, Spain

 Supplemental material for this article can be accessed [here](#).

© 2020 The Author(s). Published by Informa UK Limited, trading as Taylor & Francis Group on behalf of The International Society for Extracellular Vesicles. This is an Open Access article distributed under the terms of the Creative Commons Attribution-NonCommercial License (<http://creativecommons.org/licenses/by-nc/4.0/>), which permits unrestricted non-commercial use, distribution, and reproduction in any medium, provided the original work is properly cited.

[1,2]. IS formation is associated with an initial increase in cortical actin at the IS [3]. Subsequently, MTOC polarization is preceded by a decrease in cortical actin density at the central region of the immune synapse (cIS), that contains the secretory domain [4,5]. The central supramolecular activation cluster (cSMAC) is located in this low-density F-actin region of the cIS (Fact-Low cIS), adjacent to the secretory domain [2,4,5]. Next, cortical actin recovery at the IS leads to termination of lytic granule secretion in CTLs [6]. These reversible, cortical actin cytoskeleton reorganization processes occur during the degranulation of both the lytic granules in cytotoxic T lymphocytes (CTL) and some cytokine-containing secretory vesicles in T-helper (Th) lymphocytes [4,5,7], despite both the nature and cargo of the secretory vesicles in these cell types are quite different. Thus, the formation of a mature IS produces several crucial biological outcomes, including activation of Th cells (usually CD4<sup>+</sup> cells) and cell killing by primed CTLs (mostly CD8<sup>+</sup> cells). Accordingly, there are two major types of secretory IS established by T lymphocytes that result in very diverse, but also critical, immune effector functions [8–10]. The IS made by primed CTLs induces rapid polarization (ranging from seconds to few minutes) of the lytic granules towards the IS. The degranulation of the lytic granules induces the secretion perforin and granzymes to the synaptic cleft [11], which are pro-apoptotic molecules, but also exosomes [12]. The secreted perforin and granzymes subsequently induce killing of the target cells [13]. CTLs develop transient synapses, lasting only few minutes, as the target cells are killed [2,4]. This is probably due to the fact that the optimal CTL task requires a rapid and temporary contact with target cells, in order to distribute as many lethal strikes as possible to numerous target cells [2,4]. In contrast, Th lymphocytes such as Jurkat cells generate stable, long-standing IS (from 10–30 min up to hours), since this appears to be necessary for both directional and continuous secretion of stimulating cytokines [2,4]. Moreover, we have described in Th lymphocytes that cortical actin reorganization at the IS plays an important role during the polarized traffic of multivesicular bodies (MVB) containing intraluminal vesicles (ILV) [14], a different type of secretory vesicles involved in exosome secretion at the IS [15–17]. Exosome secretion in Th lymphocytes follows TCR stimulation, IS formation, MVB polarization and degranulation, and these exosomes can induce Fas ligand-dependent autocrine activation-induced cell death (AICD) [15,16,18], a key process in regulating T lymphocyte homeostasis [19]. Regarding the intracellular signals controlling this specialized secretory pathway, we have shown that TCR-stimulated PKC $\delta$  regulates cortical actin reorganization at the IS ultimately

controlling MTOC/MVB polarization leading to exosome secretion at the IS [14]. PKC $\delta$ -interfered T cell clones showed inhibition of cortical actin reorganization at the IS concomitantly to defective MTOC/MVB polarization [14]. Overall, this lead us to hypothesize that an altered actin reorganization at the IS may underlie the deficient MVB polarization occurring in PKC $\delta$ -interfered T cell clones [14]. However, it cannot be ruled out that PKC $\delta$  may govern other actin reorganization networks apart from actin reorganization at the IS, that may also contribute to the diminished MTOC/MVB polarization efficiency observed in PKC $\delta$ -interfered clones [14].

TCR-triggered actin cytoskeleton reorganization and polarized traffic of secretory vesicles are regulated by two major pathways: one involves HS1/WASp/Arp2/3 complexes acting in cortical F-actin, and the other formins such as formin-like 1 (FMNL1) and Diaphanous-1 (Dia1) [20,21]. Several studies suggest that cortical F-actin reorganization at the IS is necessary and sufficient for MTOC/lytic granules polarization [5,22]. However, other results show that depletion of formins FMNL1 or Dia1 impedes MTOC polarization without affecting Arp2/3-dependent cortical actin reorganization [23], supporting that, at least in the absence of FMNL1 or Dia1, cortical actin reorganization is not sufficient for MTOC polarization. Conversely, in the absence of cortical actin reorganization at the IS occurring in Jurkat cells lacking Arp2/3, the MTOC can polarize normally to the IS [21,23]. Regarding other molecules controlling MTOC polarization, paxillin (an actin-regulating adaptor protein) [24] is necessary for MTOC polarization to the IS in CTLs [25] and its phosphorylation is required for lytic granule secretion from CTL [26]. Along these lines, recent studies in B lymphocytes forming IS indicated that the MTOC is a F-actin organizing centre [27], and F-actin depletion around the MTOC crucially facilitates MTOC polarization towards the IS in B-cell receptor (BCR)-stimulated B lymphocytes [28,29]. In summary, taking together these observations, it is clear that MTOC and MVB polarization induced by IS formation are regulated by HS1/WASp/Arp2/3-dependent cortical and formin-dependent non-cortical actin networks, and that PKC $\delta$  may regulate the reorganization of both actin networks.

To better understand the mechanisms involved in these processes in T cells, we studied the contribution of FMNL1, Dia1 and paxillin. Here we report that PKC $\delta$  appears to coordinately regulate MTOC and MVB polarizations via at least two distinct actin cytoskeleton regulatory pathways: FMNL1 $\beta$ -mediated regulation of F-actin reorganization at the IS and paxillin-mediated reorganization of centrosomal area F-actin.

## Materials and methods

### Cells

Raji B and Jurkat T (clone JE6.1) cell lines were obtained from the ATCC. Cell lines were cultured in RPMI 1640 medium containing L-glutamine (Invitrogen) with 10% heat-inactivated FCS (Gibco) and penicillin/streptomycin (Gibco). Jurkat cells were transfected with control or PKC $\delta$  shRNA-encoding plasmids, selected with puromycin, and control (C3, C9) and PKC $\delta$ -interfered (P5, P6) Jurkat stable clones were isolated by limiting dilution and phenotyped as previously described [14].

### Plasmids and transient transfection

pECFP-C1 CD63 (expressing CFP-CD63) was provided by G. Griffiths. CD63 is an enriched marker in MVB and has been widely used to study the secretory traffic of MVB both in living and fixed cells [15,16]. The plasmid expressing dsRed-centrin 2 (dsRed-cent2) was a gift from J. Gleeson (Addgene plasmid # 29,523; <http://n2t.net/addgene:29523>; RRID:Addgene\_29,523). pmCherry Paxillin was a gift from K. Yamada (Addgene plasmid # 50,526; <http://n2t.net/addgene:50526>; RRID:Addgene\_50,526). The control vector (shControl-HA-YFP), FMNL1 interfering (shFMNL1-HA-YFP) and FMNL1-interfering, re-expressing vectors (shFMNL1-HA-YFP-FMNL1 $\alpha$ , shFMNL1-HA-YFP-FMNL1 $\beta$ , shFMNL1-HA-YFP-FMNL1 $\gamma$  and shFMNL1-HA-YFP-FMNL1 $\Delta$ FH2 mutant) were previously described [30] and generously provided by D. Billadeau. Jurkat clones were transiently transfected with 20–30  $\mu$ g of the plasmids as described [16].

### Antibodies and reagents

Rabbit monoclonal anti-human PKC $\delta$  EP1486Y for WB, does not recognize mouse PKC $\delta$  (Abcam). Rabbit monoclonal anti-PKC $\delta$  EPR17075 for WB recognizes both human and mouse PKC $\delta$  (Abcam). Mouse monoclonal anti-human CD3 UCHT1 for cell stimulation and immunofluorescence (BD Biosciences and Santa Cruz Biotechnology). Mouse monoclonal anti-FMNL1 clone C-5 for WB, and mouse monoclonal anti-FMNL1 clone A-4 for immunoprecipitation (Santa Cruz Biotechnology). Mouse monoclonal anti-Dia1 clone E-4 for WB (Santa Cruz Biotechnology) and rabbit polyclonal anti-Dia1 (Diap1) clone E1E4 K for immunoprecipitation (Cell Signalling Technology). Mouse monoclonal anti- $\gamma$ -tubulin for immunofluorescence (SIGMA). Mouse monoclonal anti-paxillin clone 349 for WB and anti-paxillin clone 349 coupled to TRITC for immunofluorescence (BD Biosciences). Rabbit polyclonal anti-phospho-Thr538 paxillin for WB and immunofluorescence (ECM

Biosciences). Rabbit polyclonal Phospho-(Ser) PKC substrate antibody for WB and immunofluorescence (cell signalling technology). Fluorochrome-coupled secondary antibodies (goat-anti-mouse IgG AF488 A-11029, goat-anti-rabbit IgG AF488 A-11034, goat-anti-mouse IgG AF546 A-11030, goat-anti-mouse IgG AF647 A-21236) for immunofluorescence were from ThermoFisher. Horseradish peroxidase (HRP)-coupled secondary antibodies (goat anti-mouse IgG-HRP, sc-2005 and goat anti-rabbit IgG-HRP, sc-2004) were from Santa Cruz Biotechnology. CellTracker™ Blue (CMAC) and phalloidin were from ThermoFisher. Staphylococcal enterotoxin E (SEE) was from Toxin Technology, Inc. SirActin and verapamil were from Cytoskeleton Inc.

### Immunoprecipitation

Immunoprecipitation from cell lysates was performed by using Protein A/G Magnetic Beads (Pierce, ThermoScientific) following the instructions provided by the company. Briefly, 0.5 ml lysates corresponding to 20–30  $\times 10^6$  Jurkat clones, stimulated or not as described, were incubated with the primary antibody (5  $\mu$ g) for 2 h at 4°C. Subsequently, 15  $\mu$ l of magnetic beads suspension were added and incubated for 3 h at 4°C. Beads were washed 5 $\times$  with lysis buffer and the antigens were eluted with 2 M glycine pH = 2 and neutralized. Eluates were run on SDS-PAGE gels, 6,5% Acrylamide and proteins transferred to PDVF membranes.

### Western blot analysis

Cells were lysed in Triton™  $\times 100$ -containing lysis buffer supplemented with both protease and phosphatase inhibitors. Approximately 50  $\mu$ g of cellular proteins were recovered in the 10,000 $\times$ g pellet from  $10^6$  cells. Cell lysates and neutralized, acid-eluted immunoprecipitates were separated by SDS-PAGE under reducing conditions and transferred to Hybond™ ECL™ membranes (GE Healthcare). Membranes were incubated sequentially with the different primary antibodies and developed with the appropriate HRP-conjugated secondary antibody using enhanced chemiluminescence (ECL). When required, the blots were stripped following standard protocols prior to reprobing them with primary and HRP-conjugated secondary antibodies. Autoradiography films were scanned and the bands were quantified using Quantity One 4.4.0 (BioRad) and ImageJ (Rasband, W.S., ImageJ, National Institutes of Health, Bethesda, Maryland, USA, <http://rsb.info.nih.gov/ij/>, 1997–2004) softwares.



### Time-lapse microscopy, immunofluorescence and image analysis

Jurkat clones transfected with the different expression plasmids were attached to ibidi microwell culture dishes using fibronectin (0.1 mg/ml) at 24–48 h post-transfection, and stimulated in culture medium at 37°C. In some experiments requiring IS formation, Raji cells attached to ibidi microwell culture dishes using fibronectin (ibiTreat, for paraformaldehyde fixing) or poly-L-lysine (glass bottom, for acetone-fixation) were labelled with CMAC and pulsed with 1 µg/ml SEE, mixed with transfected Jurkat clones and ISs analysed as described [15,31,32]. Acetone fixation required for  $\gamma$ -tubulin staining of MTOC was compatible with phalloidin labelling [33]. In other experiments, transfected Jurkat clones were stimulated with plastic-bound anti-TCR UCHT1 (10 µg/ml) or in suspension with phorbol myristate acetate (PMA, 100 ng/ml). Immunofluorescence of fixed synapses was performed as previously described [34], and additional fixations were performed between each fluorochrome-coupled secondary antibody staining and subsequent fluorochrome-coupled primary antibody staining, to exclude any potential cross-reaction of secondary antibodies (i.e. Figure 7a).

For in vivo actin reorganization experiments, dsRed-Cent2-transfected Jurkat clones were preincubated overnight with 100 nM SirActin and 2 µM verapamil, and subsequently challenged with SEE-pulsed Raji cells as described above. Wide-field, time-lapse microscopy was performed using an OKO-lab stage incubator (OKO) on a Nikon Eclipse TiE microscope equipped with a DS-Qi1MC digital camera and a PlanApo VC 60x/1.4NA OIL objective (Nikon). Time-lapse acquisition and analysis were performed by using NIS-AR software (Nikon). Subsequently, epi-fluorescence images were improved by Huygens Deconvolution Software from Scientific Volume Image (SVI) using the “widefield” optical option as previously described [32,35]. For quantification, digital images were analysed using NIS-AR (Nikon) or ImageJ softwares (Rasband, W.S., ImageJ, National Institutes of Health, Bethesda, Maryland, USA, <http://rsb.info.nih.gov/ij/>, 1997–2004). The quantification and analysis of F-actin mean fluorescence intensity (MFI) in a centrosome-centred area (centrosomal area F-actin MFI) in time-lapse experiments, was performed within a 2 µm diameter, floating region of interest (ROI) (i.e. ROI changing XY position over time), centred at the centre of mass of the MTOC (MTOC<sup>C</sup>), by using NIS-AR software (Figure 2d). These measurements were performed in deconvoluted time-lapse series because of the enhanced signal-to-noise ratio of the images, although

raw time-lapse series yielded comparable results. In parallel, for each time-lapse time point, the measurement of the distance from the MTOC<sup>C</sup> towards the IS was performed by using NIS-AR software and represented versus the corresponding centrosomal area F-actin MFI value (Figure 2d, upper panels). Confocal microscopy imaging of synapses made by living cells was performed by using a SP8 Leica confocal microscope equipped with an HC PL APO CS2 63x/1.2 NA water objective (zoom for C3, 5.34; zoom for P5, 4.47; scan velocity, 1000 Hz bidirectional; pixel size, 0.068 µm; pinhole, 111.5 µm; z-step size, 0.6 µm; z-stack, 9 µm). The synaptic conjugates for these experiments were prepared by mixing SEE-pulsed Raji cells with transfected Jurkat clones in suspension, as previously described [5,6]. The quantification of relative centrosomal area F-actin MFI in these experiments was calculated as the F-actin MFI corresponding to a 2 µm diameter, floating ROI, centred at the MTOC centre of mass (MTOC<sup>C</sup>), relative to the F-actin MFI of this centrosomal area ROI at time = 0, using the average intensity projection (AIP) from the three focal planes (2 µm thickness) containing the maximal signal of MTOC.

Confocal microscopy imaging in fixed synapses was performed by using a SP8 Leica confocal microscope, with sequential acquisition, bidirectional scanning and the following laser lines: UV (405 nm, intensity: 33.4%), supercontinuum visible (633 nm, intensity: 15.2%), supercontinuum visible (550 nm, intensity: 20.8%), supercontinuum visible (488 nm, intensity: 31.2%). Deconvolution of confocal images was performed by using Huygens Deconvolution Software from Scientific Volume Image (SVI) with the “confocal” optical option. Colocalization analyses were accomplished by using Jacop plugin from ImageJ.

The velocity of movement of MVB was measured by automatically analysing the trajectories of CFP-CD63<sup>+</sup> vesicles in videos (i.e. Suppl. Video 2) with the use of NIS-AR software (tracking module) and the ImageJ MJTrack plugin. The trajectory of MTOC was analysed by using ImageJ MJTrack plugin (i.e. Suppl. Video 1). In polarization experiments, to establish the relative ability of the MTOC and MVB to polarize towards the IS, MTOC and MVB polarization indexes (Pol. Indexes) were calculated as described in Figure 1a, using MIP of acetone-fixed synapses. In the MIP, the position of the cell centre of mass (Cell<sup>C</sup>), MTOC and MVB centre of mass (MTOC<sup>C</sup> and MVB<sup>C</sup>, respectively) were used to project MTOC<sup>C</sup> (or MVB<sup>C</sup>) on the vector defined by the Cell<sup>C</sup>–synapse axis. Then the MTOC (or MVB) polarization index was calculated by dividing the distance between the MTOC<sup>C</sup> (or MVB<sup>C</sup>) projection and the Cell<sup>C</sup> (“A” distance) by the distance between

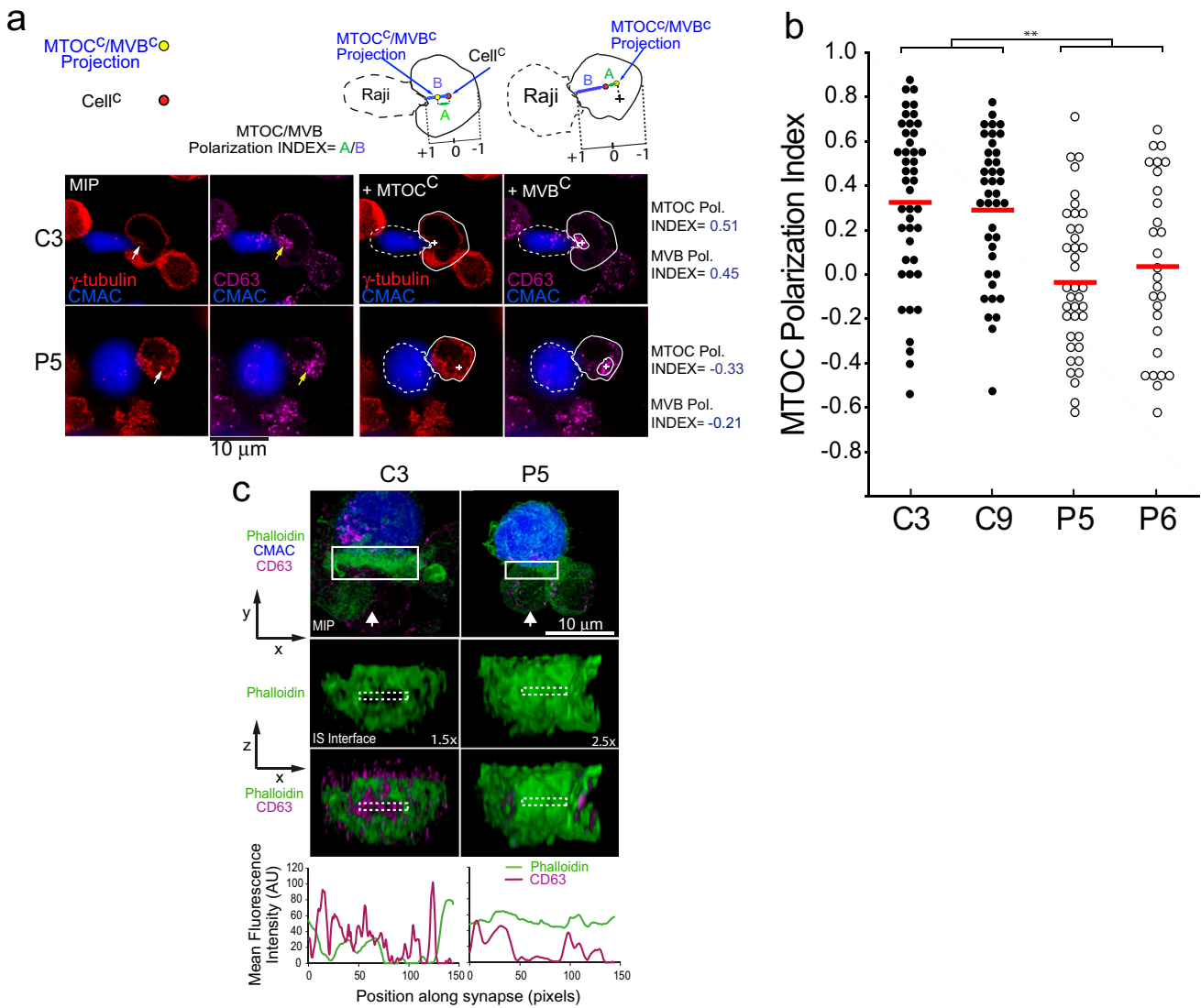


**Figure 1.** PKC $\delta$  regulates MTOC and MVB polarization.

(Panel A) C3 control and P5 PKC $\delta$ -interfered clones were challenged with CMAC-labelled SEE-pulsed Raji cells for 1 h, fixed, stained with anti- $\alpha$ -tubulin AF546 to label MTOC and anti-CD63 AF647, to label MVB and imaged by confocal fluorescence microscopy. In the upper diagram, the distances (A, green; B, blue) used for the calculation of Pol. Index (A/B) are indicated. The red dot represents the cell centre of mass (Cell<sup>C</sup>), whereas the yellow dot indicates the projection of MTOC or MVB centre of mass (MTOC<sup>C</sup> and MVB<sup>C</sup>, respectively) on the vector defined by the Cell<sup>C</sup>-synapse axis. Since the Cell<sup>C</sup> position was taken as the origin to measure distances, those "A" distance values in the opposite direction to the synapse were taken as negative. Thus, polarization indexes range from +1 (fully polarized) to -1 (fully anti-polarized). In the lower panels, MIP of the indicated, merged channels of representative images for both C3 and P5 forming synapses are included. The Raji cells and the Jurkat clones are labelled with discontinuous and continuous white lines, respectively. The superimposed white crosses label the MTOC<sup>C</sup> or MVB<sup>C</sup>. The white arrow indicates MTOC position, whereas the yellow arrow labels the MVB. (Panel B) MTOC Pol. Index was calculated as indicated in panel A for the indicated number of synaptic conjugates made by C3, C9 (control) and P5, P6 (PKC $\delta$ -interfered) clones, that were previously challenged for 1 h with SEE-pulsed Raji cells. Dot plot distribution and average Pol. Index (red horizontal line) are represented. \*\*,  $p \leq 0.05$ . (Panel C) C3 control and P5 PKC $\delta$ -interfered clones were challenged with CMAC-labelled SEE-pulsed Raji cells for 1 h, fixed, stained with phalloidin AF488 and anti-CD63 AF647 and imaged by confocal fluorescence microscopy. Upper panels: top views corresponding to the maximal intensity projection (MIP) of the indicated, three merged channels, in a representative example. White arrows indicate the direction to visualize the face on views of the synapse (IS interface) enclosed by the ROIs (white rectangles) as shown in Suppl. Video 3. Middle panels: face on views of the IS. The enlarged ROIs from the upper panel (1.5x and 2.5x zoom, respectively) were used to generate (as shown in Suppl. Video 3) the IS interface merged images (phalloidin and CD63 channels from frame no. 43 of Suppl. Video 3). Lower diagrams: phalloidin and CD63 MFI vs position along the indicated, rectangular ROIs (discontinuous line) embed in the face on views from the lower panels. CMAC labelling of Raji cells in blue, phalloidin in green and CD63 in magenta. Scale bars, 10  $\mu$ m.

the Cell<sup>C</sup> and the synapse (“B” distance) (Figure 1a). Cell<sup>C</sup> position was taken as the origin to measure distances, thus those “A” values in the opposite

direction to the synapse were taken as negative. Thus, Pol. Indexes (Pol. Index = A/B) ranked from +1 (fully polarized) to -1 (fully anti-polarized).

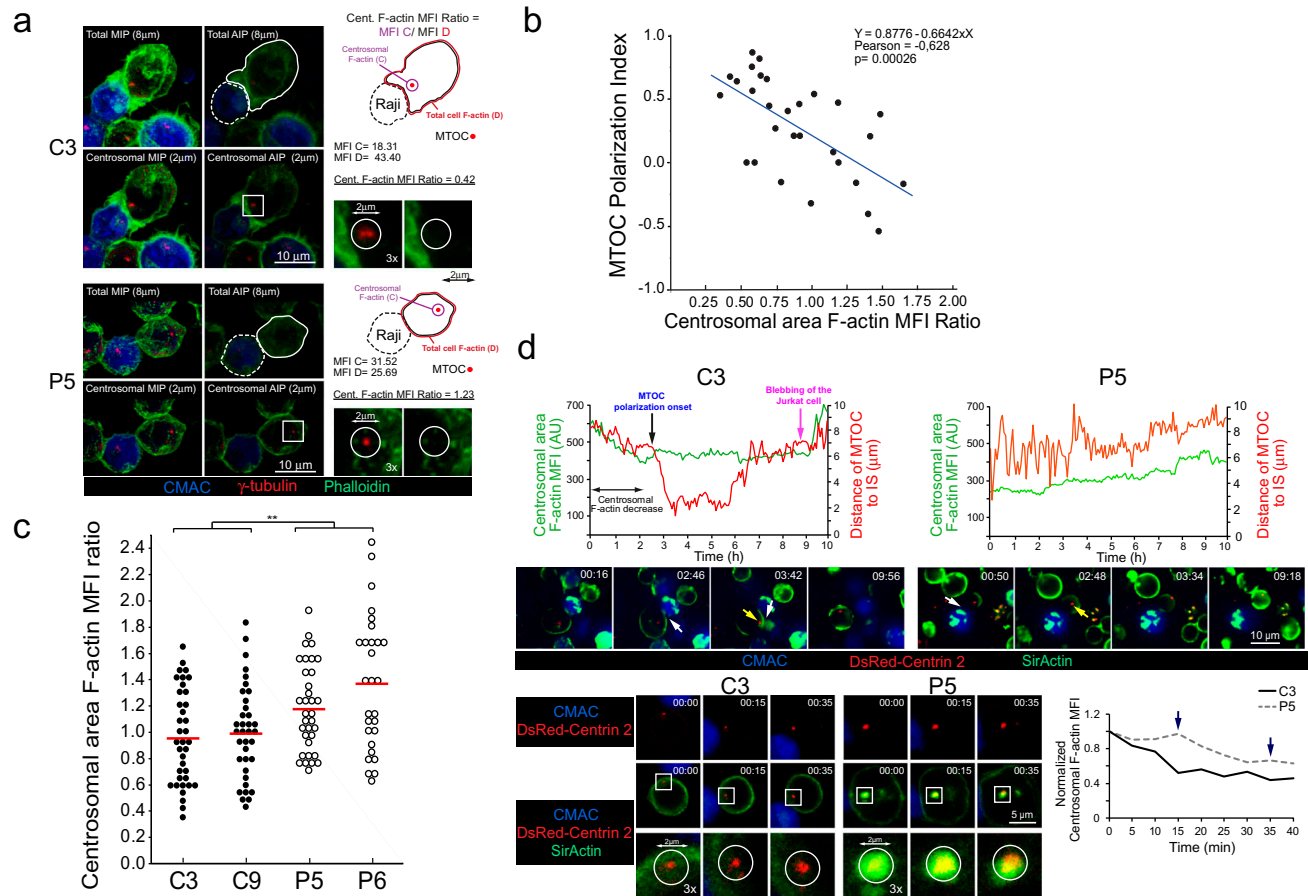


**Figure 2.** PKC $\delta$  regulates centrosomal area F-actin.

(Panel A) C3 control and P5 PKC $\delta$ -interfered clones were challenged with CMAC-labelled SEE-pulsed Raji cells for 1 h, fixed, stained with anti- $\gamma$ -tubulin AF546 to label MTOC and phalloidin AF488 to label F-actin, and imaged by confocal fluorescence microscopy. Left, total (8  $\mu$ m thick) or centrosomal (2  $\mu$ m thick), maximal or average intensity projections (MIP and AIP, respectively) are shown as indicated. In the right side images, enlarged centrosomal areas (as defined in centrosomal AIPs, white squares) are shown containing the 2  $\mu$ m-diameter centrosomal ROIs (white circles) used to calculate the centrosomal area F-actin MFI. In the right side diagrams, the F-actin MFI values in ROIs ("C" magenta ROI labels centrosomal area F-actin, whereas "D" red ROI labels total cell F-actin) used to calculate the centrosomal area F-actin MFI ratio are indicated. The Raji cells and the Jurkat clones are labelled with discontinuous and continuous lines, respectively. (Panel B) C3 control clone was challenged with CMAC-labelled SEE-pulsed Raji cells for 1 h, fixed, stained with anti- $\gamma$ -tubulin AF546 to label MTOC, and phalloidin AF488 to label F-actin and imaged by confocal fluorescence microscopy. Subsequently, centrosomal area F-actin MFI ratio and MTOC polarization index were calculated as indicated in Material and Methods, linear correlation analyses between these values corresponding to each individual cell was represented and Pearson's correlation coefficient was calculated. Non-parametric Spearman's correlation  $\rho = -0.633$  ( $p = 0.00017$ ). (Panel C) Centrosomal area F-actin MFI ratio was calculated for synaptic conjugates made by C3, C9 (control) and P5, P6 (PKC $\delta$ -interfered) clones as indicated in panel A. Dot plot distribution and average centrosomal area F-actin MFI ratio (red horizontal line) are represented. \*\*,  $p \leq 0.05$ . (Panel D) Upper diagrams, C3 control and P5 PKC $\delta$ -interfered clones expressing dsRed-Cent2 and pulsed with SirActin and verapamil were challenged with CMAC-labelled SEE-pulsed Raji cells bound to glass-bottom plates. Subsequently, synapses were imaged by wide-field, time-lapse microscopy and centrosomal area F-actin MFI (green line) and the distance of the MTOC to the IS (red line) were measured in each frame, as indicated in Materials and Methods, using a 2  $\mu$ m-diameter floating ROI, centred at the MTOC<sup>C</sup>. Vertical black arrow labels the onset of MTOC polarization, whereas magenta arrow labels the blebbing of the Jurkat clone at late time points. Horizontal double-arrow line labels the time period during which centrosomal area F-actin decreased. Middle panels, some representative frames of the indicated, merged channels (CMAC, blue; dsRed-Cent2, red; SirActin, green) are included (see also Suppl. Video 4). White arrow labels the synapse, whereas yellow arrow labels the MTOC. Lower panels, C3 control and P5 PKC $\delta$ -interfered clones expressing dsRed-Cent2 and pulsed with SirActin and verapamil were challenged with CMAC-labelled SEE-pulsed Raji cells in suspension. Subsequently, synapses were imaged by confocal time-lapse microscopy and centrosomal area F-actin MFI was measured, using a 2  $\mu$ m-diameter floating ROI centred at the MTOC<sup>C</sup>, as indicated in Materials and Methods. Left panels include some representative frames of the merged channels (CMAC, blue; dsRed-Cent2, red; SirActin, green, see also Suppl. Video 5), whereas the right diagram represents the kinetics of normalized centrosomal area F-actin MFI (referred to MFI at  $t = 0$ ). Dark arrows indicate the representative frames shown in the left panels. The slow decrease in centrosomal area F-actin MFI occurring in P5 clone, which was not evident in the epi-fluorescence experiment shown in the upper plot, is due to the increased fluorescence bleaching by the confocal illumination conditions. Data are representative of the results obtained in several experiments ( $n = 3$ ).

Therefore Pol. Index values were normalized by cell size and shape (Figure 1a). For the experiments analysing F-actin reorganization at MTOC area in fixed cells, the MTOC area-associated F-actin (centrosomal area F-actin) was quantified by labelling MTOC with  $\gamma$ -tubulin or expressing dsRed-Cent2, since both labelling approaches rendered equivalent results, as shown in Figure 2 and Suppl. Fig. S3. Briefly, after manual selection of the z optical section containing the maximal signal corresponding to the centrosome ( $\gamma$ -tubulin or dsRed-Cent2 signal), a substack (2  $\mu$ m thickness) centred at the MTOC<sup>c</sup> was selected, and the F-actin average intensity z-projection (AIP) of the substack was generated (centrosomal area AIP) and thresholded (Default), by using ImageJ. Subsequently, a circular ROI “C” (2  $\mu$ m diameter) centred at the MTOC<sup>c</sup> was selected on the thresholded, centrosomal area AIP, and the F-actin MFI in this ROI was calculated, and this value corresponded to centrosomal area F-actin MFI (MFI in ROI “C”, Figure 2a and Suppl. Fig. S3). In parallel, we calculated the cellular F-actin MFI of the thresholded (Default) average intensity z-projection (AIP) corresponding to all focal planes (total AIP), using a ROI including the whole cell (MFI in ROI “D”, Figure 2a and Suppl. Fig. S3). We then calculated the centrosomal area F-actin MFI ratio (centrosomal area F-actin MFI/cell F-actin MFI = MFI C/MFI D) to normalize by cell size and by phalloidin labelling among different samples. This value represented the relative density of centrosomal area F-actin (Figure 2, Suppl. Fig. S3). For paxillin phosphorylation image analyses, image quantification of phospho-T538 MFI signal in fixed synapses was performed by using ROI defined with the “autodetect” algorithm from NIS-AR, containing the paxillin fluorescence signal. These phospho-T538 MFI values were internally normalized by paxillin MFI values in the same ROI by using ImageJ. For image analyses of FMNL1 isoform phosphorylation, image quantification of Phospho-(Ser) PKC substrate signal was performed by using cell ROIs defined with the “Autodetect” algorithm from NIS-AR and an appropriate threshold. Image analysis data correspond to at least three different experiments, analysing a minimum of 30 synapses from 15 different, randomly selected, microscopy fields per experiment. ANOVA analysis was performed for statistical significance of the results using Excel and IBM’s SPSS Statistics software.

## Results

### *PKC $\delta$ interference decreases both MTOC and MVB polarization towards the IS*

We have previously shown, by using a well-established IS model [31,32,35], that PKC $\delta$ -interfered Jurkat clones challenged with antigen on APC secreted a lower amount of exosomes upon IS formation [14]. We also defined that the deficient polarization of MVB containing the exosome precursors towards the IS underlies the decreased exosome secretion [14]. In the context of secretory traffic at the IS, it has been published that not always MTOC polarization is necessary or sufficient for the transport or certain secretory vesicles to the IS [7], such as lytic granules, and for the cytotoxic hit delivery [36–38]. All these previous examples of segregation between MTOC movement and secretory granules traffic prompted us to simultaneously analyse both MTOC and MVB movement at the single cell level. We first analysed by time-lapse microscopy MTOC polarization, MVB convergence towards the MTOC and MVB polarization in Jurkat clones co-expressing dsRed-Cent2 and CFP-CD63, upon challenge with SEE-pulsed Raji cells, which is a well-established Th synapse model [31]. As shown in the representative Suppl. Video 1, MVB convergence towards the MTOC occurred almost simultaneously with MTOC migration towards the IS. We then quantitated MTOC and MVB polarization in fixed synapses formed by control or PKC $\delta$ -interfered Jurkat clones by fluorescence microscopy, as previously described [14] (Figure 1a). As seen in Figure 1b, C3 and C9 control clones substantiated significantly higher MTOC polarization indexes when compared to P5 and P6 PKC $\delta$ -interfered clones. We have previously compared MVB polarization indexes among these clones obtaining comparable results [14]. Remarkably, we found a strong linear correlation between MVB and MTOC polarization indexes (Pol. Index) for each clone (i.e. Pearson’s linear correlation coefficient 0.962 and 0.949 for C3 and P5 clones, respectively, Suppl. Fig S1), accordingly with the Suppl. Video 1. Furthermore, in all the analysed synapses the MTOC<sup>c</sup> was coincident or very proximal to the MVB<sup>c</sup> (i.e. Suppl. Video 1, Figure 1a), regardless of polarization. Although the MTOC and MVB did not efficiently polarize in P5 and P6 PKC $\delta$ -interfered cells (Figure 1), their MVB still converged towards the MTOC (Figure 1a, Suppl. Fig. S1). Thus, PKC $\delta$  appears to specifically regulate MTOC movement to the IS.



### ***PKC $\delta$ regulates F-actin reorganization at the IS and around the MTOC during MTOC polarization***

Our previous results show that PKC $\delta$  regulates cortical F-actin reorganization at the IS, contributing to MVB polarization and exosome secretion [14], since PKC $\delta$ -interfered clones forming synapses exhibited quantitative alterations (duration and magnitude of F-actin reorganization), but also qualitative differences (absence of depletion of F-actin at the cIS) in F-actin reorganization at the IS when compared with control clones [14]. All these defects were rescued by ectopic, mouse PKC $\delta$  re-expression in PKC $\delta$ -interfered clones, as well as the defective MTOC/MVB polarization [14]. We aimed to explore the consequences of this defective cortical F-actin reorganization on MTOC/MVB polarization. To this end, we labelled C3 control and P5 PKC $\delta$ -interfered clones with phalloidin and anti-CD63, to visualize in the same cell F-actin and MVB, respectively, by confocal microscopy. We then analysed the 3D distributions of F-actin and MVB and generated 2D projections of both distributions at the IS interface (Suppl. Video 3 and Figure 1c, medium and lower panels). Next, to evaluate the relative position of CD63<sup>+</sup> vesicles (MVB) with respect to F-actin architecture at the IS, the MFI of F-actin and CD63 along the IS interface (ROI labelled with discontinuous white-line rectangles in Figure 1c) was measured (Figure 1c, bottom diagrams). In C3 control clone we found an accumulation of MVB (peaks in the magenta MFI profile, lower panels) included in the F-actin-depleted area (represented by a valley in the green MFI profile) at the cIS (Figure 1c), that includes the secretory domain [4]. In contrast, in P5 PKC $\delta$ -interfered clone, neither the F-actin-depleted area nor MVB were observed at the cIS (Figure 1c). Thus, cortical F-actin reorganization at the IS is regulated by PKC $\delta$ , and this reorganization appears to control MVB polarization and hence MVB secretion. In addition, when we expressed dsRed-Cent2 in Jurkat clones to assess MTOC position in relation to the F-actin depleted area at the cIS, we found in C3 control clone the MTOC located at the edge of the cIS (Suppl. Fig. S2, yellow arrow in upper left panel) that corresponded to the described secretory domain next to the cSMAC [4], in accordance with the observed MVB position (Figure 1c). However, in P5 PKC $\delta$ -interfered clone, the MTOC position was distal to the IS (Suppl. Fig. S2, yellow arrow in right panel). Thus, the spatial organization of F-actin at the IS is altered in PKC $\delta$ -interfered clones, and this may contribute to the deficient MTOC/MVB

polarization, although at this stage we could not exclude that other non-cortical F-actin-dependent events may also contribute to the observed phenotype.

In this context, it has been demonstrated that F-actin depletion at a 2  $\mu$ m-diameter centrosomal area appears to be crucial to allow MTOC polarization towards the IS in BCR-stimulated B lymphocytes [28]. However, to date no evidence of centrosomal area F-actin depletion has been reported during MTOC polarization in T lymphocytes. We thus analysed centrosomal area F-actin in T lymphocytes in a control clone forming synapses. To perform these experiments we measured thresholded, F-actin MFI within a defined, spherical ROI (2  $\mu$ m diameter) centred at the MTOC<sup>c</sup>, as previously described [28], and we divided this centrosomal area F-actin MFI by total cellular F-actin MFI, to normalize by cell area, shape and phalloidin staining variations among samples (Figure 2a, upper panels). The possible correlation of the centrosomal area F-actin MFI ratio with the MTOC polarization index was analysed in C3 control (Figure 2b) and P5 PKC $\delta$ -interfered (not shown) clones. A negative correlation was observed in the C3 control clone (Spearman's Rho Coefficient =  $-0.632$ ;  $p = 0.00017$  and Pearson's Coefficient =  $-0.628$ ;  $p = 0.00026$ ), but no correlation was observed (Spearman's Rho Coefficient =  $-0.13$ ;  $p = 0.44$  and Pearson's Coefficient =  $-0.2$ ;  $p = 0.22$ ) in the P5 PKC $\delta$ -interfered clone. Moreover, when we compared control and PKC $\delta$ -interfered clones forming synapses in end point experiments, we found a statistically significant higher centrosomal area F-actin MFI ratio in PKC $\delta$ -interfered clones (Figure 2a and 2c). Thus, PKC $\delta$ -interfered clones forming synapses exhibited higher levels of centrosomal area F-actin.

The asynchronous character of synapse formation may also lead to asynchronous MTOC polarization [14,35,39], that may in turn skew the results from end point, fixed synapses. To circumvent this caveat, we first analysed by epifluorescence and subsequent image deconvolution, the centrosomal area F-actin reorganization upon synapse formation by time-lapse analyses at the single, living-cell level. To correlate centrosomal area F-actin with MTOC polarization we performed these experiments with clones expressing dsRed-Cent2 [39], loaded with SirActin and verapamil [40] and subsequently challenged with SEE-pulsed Raji cells. As seen in Figure 2d and Suppl. Video 4, upon the synaptic contact of C3 control clone (white arrow in Suppl. Video 4), concomitantly with the initial increase in cortical F-actin MFI at the IS [14] (Suppl. Video 4 and Figure 2d, white arrow in the middle panel), a progressive decrease of centrosomal area F-actin MFI (labelled by

a double arrow line in Figure 2d, upper left panel) was observed, which represented centrosomal area F-actin dismantling. Neither centrosomal area F-actin dismantling nor MTOC polarization occurred in control clones not forming synaptic conjugates (not shown). Remarkably, the early decrease in centrosomal area F-actin MFI occurred before the onset of the rapid polarization of MTOC towards the IS (black vertical arrow in Figure 2d, upper-left panel). This was consistent with the hypothesized role of centrosomal area F-actin dismantling in MTOC polarization. At late time points (magenta arrow in Figure 2d and Suppl. Video 4), plasma membrane blebbing (an early feature of T lymphocyte AICD) occurred in the C3 control clone forming synapse, as previously shown [14,15,17]. Centrosomal area F-actin dismantling did not occur in the P5 PKC $\delta$ -interfered clone, since centrosomal area F-actin MFI was maintained (Figure 2d, upper-right panel), concomitantly with the absence of MTOC polarization (yellow arrow in Suppl. Video 4, lower panels, and right-middle panel in Figure 2d) and no AICD occurred (Suppl. Video 4). End point analyses of centrosomal area F-actin and MTOC polarization in dsRed-Cent2-expressing clones rendered similar results to those obtained by labelling MTOC with anti- $\gamma$ -tubulin (compare Suppl. Fig. S3 with Figure 2a and 2c). In addition, to enhance the spatial resolution we performed shorter time-lapse analyses but using confocal microscopy. As seen in Suppl. Video 5, the P5 PKC $\delta$ -interfered clone forming synapses exhibited higher levels of centrosomal area F-actin than the C3 control clone (Figure 2d, lower right panel). Centrosomal area F-actin partially overlapped with dsRed-Cent2 in the P5 PKC $\delta$ -interfered clone, but not in the C3 control clone (Figure 2d, lower left panel). The high centrosomal area F-actin green fluorescence partially overlapped the dsRed-Cent2 red fluorescence at MTOC, rendering an evident yellow dot in the P5 clone (Figure 2d, lower left panel). Thus, centrosomal area F-actin dismantling correlated with MTOC polarization to the IS and, since PKC $\delta$ -interfered clones exhibited sustained levels of centrosomal area F-actin, PKC $\delta$  appeared to negatively regulate this process.

### **FMNL1 colocalizes with F-actin at the IS but not around the MTOC**

FMNL1 is required for MTOC polarization in T lymphocytes and this event appears to be independent of Arp2/3-mediated, cortical F-actin reorganization at the IS [23]. In PKC $\delta$ -interfered clones we have observed that the spatial F-actin organization at the IS is affected, but also the centrosomal area F-actin reorganization (see above). Thus, it is conceivable that PKC $\delta$  may exert its regulatory role on MTOC polarization via regulation of FMNL1 function acting

separately and/or coordinately in any of these subcellular localizations. FMNL1 is located at the IS and around the MTOC [23] and PKC $\delta$  is located around the MTOC [14]. As a first approach to understand the molecular bases of PKC $\delta$  effect on the different, subcellular F-actin networks, we studied subcellular localization of FMNL1 in relation to F-actin cytoskeleton at both the IS and centrosomal area. As shown in Figure 3a-b, FMNL1 and F-actin partially colocalized at the IS, similarly in C3 control and P5 PKC $\delta$ -interfered clones (Figure 3b). In addition, no colocalization of FMNL1 and F-actin was observed around the MTOC either in the C3 or the P5 clone (Figure 3b and Suppl. Fig. S4).

### **PKC $\delta$ induces FMNL1 phosphorylation**

Since no differences in the subcellular localization of FMNL1 with respect to F-actin between control and PKC $\delta$ -interfered clones were observed, and all the clones exhibited similar levels of FMNL1 and Dia1 (Figure 4, upper panel and Suppl. Fig. S5), we aimed to search for potential post-translational modifications in FMNL1 and Dia1, such as phosphorylation, which may underlie the observed phenotype. FMNL2 is phosphorylated by PKC $\alpha$  and, to a lower extent, by PKC $\delta$  at S1072 [41], reversing its autoinhibition by the C-terminal, DAD auto-inhibitory domain and enhancing F-actin assembly,  $\beta$ 1-integrin endocytosis, and invasive motility [41]. In FMNL1 $\beta$ , S1086 is surrounded by a sequence displaying high homology to the one surrounding S1072 of FMNL2, whereas the homology of FMNL1 $\alpha$  and FMNL1 $\gamma$  with the C-terminus of FMNL2 was much lower [42] [41] (Suppl. Fig. S6). In addition, the three FMNL1 isoforms share identical sequence from amino acid residue 1–1070, and diverge in the C-terminal region, which includes the DAD auto-inhibitory domain (Suppl. Fig. S6). Thus, PKC $\delta$  may regulate F-actin reorganization by controlling FMNL1 $\beta$  S1086 phosphorylation, as certain PKC isoforms regulate FMNL2 activity [41]. We immunoprecipitated FMNL1 from C3 control and P5 PKC $\delta$ -interfered clones, untreated or treated with PKC activator PMA or anti-TCR, and analysed FMNL1 phosphorylation in the immunoprecipitates by WB with anti-Phospho-(Ser) PKC substrate antibody [41]; the results were normalised by FMNL1 levels in the immunoprecipitates. As shown in Figure 4a, both PMA and anti-TCR stimulation-induced FMNL1 phosphorylation in the C3 control clone to a higher extent than in the P5 PKC $\delta$ -interfered clone. Moreover, expression of an interference-resistant, GFP-PKC $\delta$  in the P5 PKC $\delta$ -interfered clone restored the phosphorylation of FMNL1 to the levels found in the C3 control clone (Figure 4b). In contrast, when we analysed in parallel Dia1 phosphorylation using the same anti-

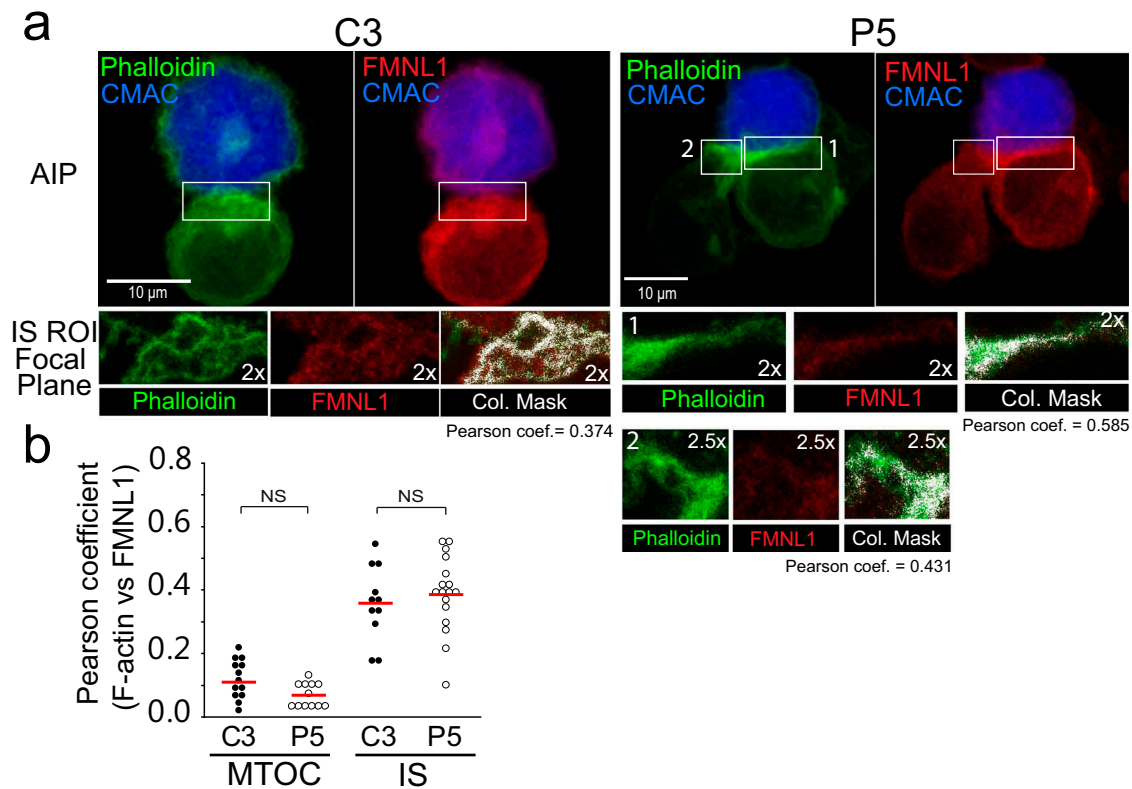


**Figure 3.** Subcellular localization of FMNL1.

C3 control (left) and P5 PKC $\delta$ -interfered clones (right) were challenged with CMAC-labelled SEE-pulsed Raji cells for 1 h, fixed, stained with anti-FMNL1 AF546 and phalloidin AF488 to label F-actin, and imaged by confocal fluorescence microscopy. (Panel A) In the upper panels, representative average intensity projections (AIP) of the indicated, merged channels of synaptic conjugates made by C3 (left panels) and P5 (right panels) clones are shown. White rectangles enclosed the IS ROIs used for the colocalization analyses of the indicated channels in the optical sections represented in the lower row of panels. In the right side of this row, colocalization masks corresponding to merged, phalloidin and FMNL1 channels, are represented in white. Pearson's coefficients corresponding to each colocalization analysis are indicated below each colocalization mask panel. CMAC labelling of Raji cells in blue, phalloidin in green and FMNL1 in red. (Panel B) same as panel A, but colocalization analyses were performed for both centrosomal, MTOC ROI (see also Suppl. Fig. S4) and IS ROI in both C3 control and P5 PKC $\delta$ -interfered clones. Dot plot distribution represents the Pearson's coefficients corresponding to each colocalization analysis and to each clone. Data are representative of the results obtained in several experiments ( $n = 3$ ). NS, not significant.

Phospho-(Ser) PKC substrate antibody, we could not detect any phosphorylation of Dia1 induced by PMA in the Dia1 immunoprecipitates (Suppl. Fig. S5). Thus, PKC isoforms activated by PMA (including PKC $\delta$ ) appear to regulate FMNL1, but not Dia1, phosphorylation. Since expression of an interference-resistant GFP-PKC $\delta$  restored FMNL1 phosphorylation (Figure 4b) and MTOC polarization [14], all these data indicate that PKC $\delta$  regulates phosphorylation of FMNL1 and probably its function during MTOC polarization.

### FMNL1 $\beta$ phosphorylation and MTOC polarization

The previous results suggest that PKC $\delta$ -dependent phosphorylation of FMNL1 may regulate FMNL1 function on F-actin reorganization at the IS and hence affect MTOC polarization. It has been shown that FMNL1 interference impedes MTOC polarization [23]. Jurkat cells contain

three FMNL1 isoforms ( $\alpha$ ,  $\beta$  and  $\gamma$ ) [30] and the antibody we used for IP recognizes all these isoforms. Thus, any of these isoforms may be phosphorylated and/or involved in F-actin reorganization and hence MTOC polarization. To investigate the contribution of FMNL1 isoforms in MTOC polarization, we transfected the C3 control and P5 PKC $\delta$ -interfered clones with a bi-cistronic YFP expression plasmid interfering all FMNL1 isoforms (shFMNL1-HA-YFP) [30]. We then challenged the clones with SEE-pulsed Raji cells and analysed MTOC polarization in non-transfected (NT, YFP $^-$ ) cells and FMNL1-interfered (YFP $^+$ ) cells. As seen in Figure 5a, the transient interference of all FMNL1 isoforms decreased the efficiency of MTOC polarization with respect to non-transfected C3 control cells forming synapses. However, it is noteworthy that FMNL1 interference did not further decrease MTOC polarization in the P5 PKC $\delta$ -interfered clone (Figure 5b), which is compatible with PKC $\delta$  and FMNL1 being in the same regulatory

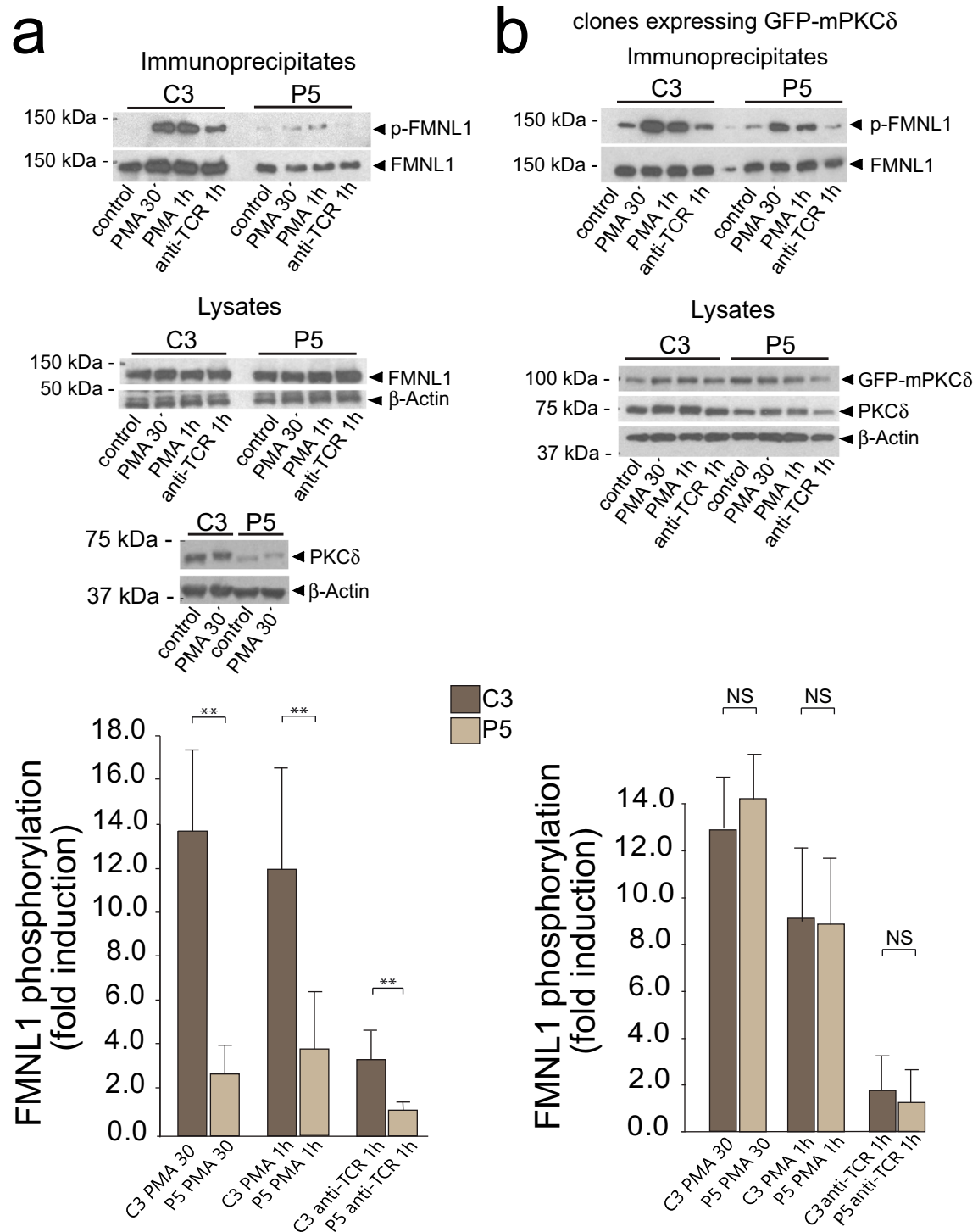


**Figure 4.** PKC $\delta$  regulates FMNL1 phosphorylation.

(Panel A), C3 control and P5 PKC $\delta$ -interfered clones were untreated or stimulated with either PMA or plastic-bound anti-TCR and subsequently lysed. WB of anti-FMNL1 immunoprecipitates (IPs) (upper panel) and cell lysates (lower panel) were sequentially probed with anti-Phospho-(Ser) PKC substrate and anti-FMNL1, to normalize Phospho-(Ser) PKC substrate signal for FMNL1 content in the IPs. In addition, cell lysates were probed with anti-FMNL1,  $\beta$ -actin and PKC $\delta$  (to check PKC $\delta$  interference). In the lower bar graph, the fold induction of FMNL1 phosphorylation, normalized to FMNL1 levels, was evaluated by WB quantification of several experiments similar to that described in the upper panel. Data are means plus SD of the results obtained in several ( $n = 5$ ) experiments. \*\*,  $p \leq 0.05$ . (Panel B), C3 control and P5 PKC $\delta$ -interfered clones were transfected with an interference resistant, GFP-mPKC $\delta$  expression plasmid. Subsequently, cells were stimulated as in panel A, and the anti-FMNL1 immunoprecipitates analysed by WB with anti-Phospho-(Ser) PKC substrate and anti-FMNL1, to normalize Phospho-(Ser) PKC signal for FMNL1 content in the IPs. In addition, the cell lysates were probed with anti-FMNL1, anti- $\beta$ -actin and anti-panPKC $\delta$ , to check for both PKC $\delta$  interference and GFP-mPKC $\delta$  expression. In the lower bar graph, the fold induction of FMNL1 phosphorylation in cells expressing GFP-mPKC $\delta$ , normalized to FMNL1 levels, was evaluated by WB quantification of several experiments similar to that described in the upper panel. Data are means plus SD of the results obtained in several ( $n = 5$ ) experiments. NS, not significant; \*\*,  $p \leq 0.05$ .



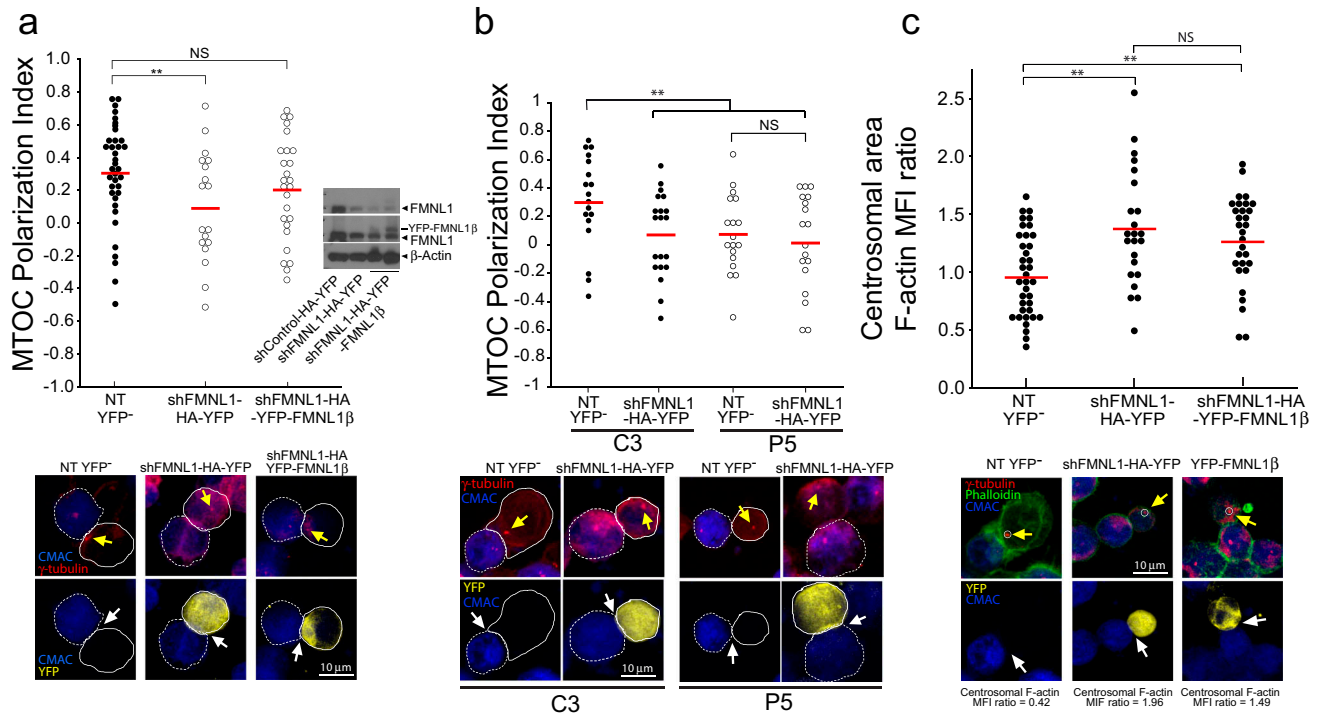


**Figure 5.** FMNL1 interference affects both centrosomal area F-actin and MTOC polarization. FMNL1β regulates MTOC polarization.

C3 control and P5 PKCδ-interfered clones were transfected with either control (shControl-HA-YFP), FMNL1 interfering (shFMNL1-HA-YFP), or FMNL1-interfering, YFP-FMNL1β expressing vector (shFMNL1-HA-YFP-FMNL1β). Subsequently, the transfected clones were challenged with CMAC-labelled SEE-pulsed Raji cells for 1 h, fixed, stained with anti-γ-tubulin AF546 (red) and phalloidin AF647 (green) to label F-actin, and imaged by confocal fluorescence microscopy. Yellow channel fluorescence identifies the transfected cells. Panel A, upper diagram, MTOC Pol. Index was calculated as indicated above, for the indicated number of synaptic conjugates made by C3 control clone, transfected or not (NT YFP<sup>-</sup> cells). Dot plot distribution and average Pol. Index (red horizontal line) are represented. In the inset, WB of cell lysates from the different groups of cells used was developed with anti-FMNL1 (two different expositions) and anti-β-actin to check for both FMNL1 interference and HA-YFP-FMNL1β expression. Lower panels, representative synapses made by C3 clone, transfected or not (NT YFP<sup>-</sup>). This group includes all non-transfected cells from both shFMNL1-HA-YFP and shFMNL1-HA-YFP-FMNL1β-transfections as internal controls. AIPs of the indicated, merged channels for C3 clone forming synapses are represented. Raji cells and Jurkat clones are labelled with discontinuous and continuous white lines, respectively. Panel (b), upper diagram, MTOC Pol. Index was calculated as indicated in Figure 1, panels A and B, for the synaptic conjugates made by C3, (control) and P5 (PKCδ-interfered) clones, transfected or not (NT YFP<sup>-</sup>). Dot plot distribution and average Pol. Index (red horizontal line) are represented. Lower panels, representative synapses made by the different clones, transfected or not (NT YFP<sup>-</sup>). AIPs of the indicated, merged channels for both C3 and P5 clones forming synapses are represented. White arrows indicate the synaptic area, whereas yellow arrows indicate the MTOC position. Panel C, upper diagram, centrosomal area F-actin MFI ratio was calculated as indicated in Figure 2 for the indicated number of synaptic conjugates made by C3 control clone, transfected or not (NT YFP<sup>-</sup>). The mean centrosomal area F-actin MFI ratio (red horizontal line) for each condition is represented. Lower panels, representative synapses made by C3 clone, transfected or not (NT YFP<sup>-</sup>). AIPs of the indicated, merged channels for C3 clone forming synapses are represented. The centrosomal area F-actin MFI ratio value is indicated for each condition. The MTOC is labelled with yellow arrow and the synapses with white arrows. The white circle enclosing the MTOC labels the ROI used to calculate the centrosomal F-actin MFI. NS, not significant. \*\*,  $p \leq 0.05$ .

pathway. We then transfected the C3 control clone with either a plasmid interfering all FMNL1 isoforms (shFMNL1-HA-YFP) or a plasmid interfering all FMNL1 isoforms and expressing interference-resistant FMNL1β (shFMNL1-HA-YFP-FMNL1β). YFP-FMNL1β expression rescued the defective MTOC polarization occurring in FMNL1-interfered cells (Figure 5a) but it was not able to decrease the high levels of the centrosomal area F-actin to control levels (Figure 5c). This suggests that, at least in conditions where all the FMNL1 isoforms, excluding FMNL1β, are interfered, centrosomal area F-actin decrease does not appear to be an absolute requirement for MTOC

polarization. In addition, expression of interference-resistant FMNL1α (shFMNL1-HA-YFP-FMNL1α) or FMNL1γ (shFMNL1-HA-YFP-FMNL1γ) did not rescue the MTOC polarization to control levels (Suppl. Fig. S7), supporting a specific role of FMNL1β in MTOC polarization. Moreover, expression of FMNL1α or FMNL1γ was unable to rescue the centrosomal area F-actin to control levels (Suppl. Fig. S8), as it occurred with FMNL1β.

To explore the contribution of cortical actin reorganization to MTOC polarization in these conditions, F-actin architecture at the cIS was analysed. Depletion of F-actin at cIS in FMNL1-interfered cells was lower than in non-

transfected cells (Suppl. Fig. S9), as occurs in PKC $\delta$ -interfered cells [14], and FMNL1 $\beta$  re-expression rescued the F-actin depletion at the cIS (Suppl. Fig. S9). Thus, in these cells, FMNL1 $\beta$  acting on cortical F-actin appears to be sufficient for MTOC polarization, despite of the high levels of centrosomal area F-actin.

FMNL1 $\beta$  is a strong candidate to be regulated by PKC $\delta$ -mediated phosphorylation (see above). To test this hypothesis, we first analysed unstimulated or PMA-stimulated, HA-YFP-FMNL1 $\beta$ -transfected C3 control cells by immunofluorescence with the anti-Phospho-(Ser) PKC substrate antibody. The low transfection efficiency of the FMNL1 constructions (less than 10% of cells expressed the FMNL1 isoforms) made unfeasible the quantitative immunoprecipitation of these isoforms. Thus, strictly controlled, single-cell image analyses of Phospho-(Ser) PKC-substrate fluorescence signal were required to address FMNL1 isoforms phosphorylation. PMA increased the Phospho-(Ser) PKC-substrate MFI signal in YFP-FMNL1 $\beta^+$  cells with respect to YFP $^-$  cells (Suppl. Fig. S10A), but this increase did not occur in HA-YFP-FMNL1 $\alpha$ , HA-YFP-FMNL1 $\gamma$  or HA-YFP-FMNL1 $\Delta$ FH2 mutant (a deletion mutant lacking the C-terminal region including the S1086)-expressing cells (Suppl. Fig. S10B). The same analysis was performed for unstimulated or PMA-stimulated, HA-YFP-FMNL1 $\beta$ -transfected C3 control and P5 PKC $\delta$ -interfered cells and the anti-Phospho-(Ser) PKC-substrate signal in PMA-stimulated C3 control cells was significantly higher than in PMA-stimulated P5 PKC $\delta$ -interfered cells (Figure 6a). Moreover, a linear correlation was observed between HA-YFP-FMNL1 $\beta$  expression and anti-Phospho-(Ser) PKC-substrate labelling in PMA-stimulated HA-YFP-FMNL1 $\beta$ -expressing, C3 control cells, and this correlation was not observed in PMA-stimulated, HA-YFP-FMNL1 $\beta$ -expressing P5 PKC $\delta$ -interfered cells (Suppl. Fig. S10 C). In addition, colocalization of HA-YFP-FMNL1 $\beta$  and anti-Phospho-(Ser) PKC substrate signals was observed in PMA-stimulated HA-YFP-FMNL1 $\beta$ -expressing C3 control cells (Pearson coefficient >0.90, not shown). All these results, together with the fact that FMNL1 has no kinase activity, support a deficient specific phosphorylation of HA-YFP-FMNL1 $\beta$  in PMA-stimulated, PKC $\delta$ -interfered cells. In addition, the increase in anti-Phospho-(Ser) PKC substrate signal triggered by IS formation in HA-YFP-FMNL1 $\beta$ -expressing, C3 control cells was higher than in YFP $^-$ , C3 control cells (Suppl. Fig. S10D). The anti-Phospho-(Ser) PKC-substrate signal in HA-YFP-FMNL1 $\beta$ -expressing, P5 PKC $\delta$ -interfered cells forming synapses was lower than in HA-YFP-FMNL1 $\beta$ -expressing, C3 control cells forming synapses (Figure 6b). To support that part of the anti-Phospho-(Ser) PKC-substrate signal indeed corresponded to the phosphorylation of HA-YFP-FMNL1 $\beta$ , we performed a colocalization analysis and

found that HA-YFP-FMNL1 $\beta$ , but not HA-YFP-FMNL1 $\alpha$ , partially colocalized with the anti-Phospho-(Ser) PKC substrate signal at the IS (Figure 6c). As an internal colocalization positive control we determined the Pearson colocalization coefficient of HA-YFP-FMNL1 $\beta$  versus anti-FMNL1 (>0.80, not shown). Thus, PKC $\delta$  interference appeared to specifically inhibit FMNL1 $\beta$  phosphorylation.

### **PKC $\delta$ induces paxillin phosphorylation at the MTOC**

The results from the previous section suggest that PKC $\delta$ -mediated FMNL1 $\beta$  phosphorylation at the IS may underlie F-actin reorganization at the IS, contributing to MTOC polarization. Although PKC $\delta$  appears to regulate centrosomal area F-actin (Figure 2c), FMNL1 $\beta$  does not appear to participate in this regulation (Figure 5c). A possible downstream effector of PKC $\delta$  in centrosomal area F-actin reorganization could be the actin regulatory protein paxillin, whose phosphorylation at threonine 538 (T538) by PKC $\delta$  leads to the depolymerization of the actin cytoskeleton and regulates integrin-mediated adhesion and migration of B lymphoid cells [43]. Moreover, the MTOC cannot polarize to the IS in paxillin-interfered T lymphocytes [25]. In addition, paxillin phosphorylation is required for the degranulation of CTL [26]. To analyse the subcellular location of paxillin with respect to MVB/MTOC polarization we first co-expressed GFP-actin, CFP-CD63 and Cherry-paxillin in C3 control and P5 PKC $\delta$ -interfered Jurkat clones, challenged them with SEE-pulsed Raji cells and analysed by time-lapse microscopy the subcellular localization of paxillin relative to the reorganization of cortical actin and MVB polarization upon IS formation. We observed that Cherry-paxillin exhibited a mainly diffuse cytosolic distribution as well as decorated punctate structures nearby the MVB (Suppl. Video 6). In the C3 control clone, these structures polarized together with MVB towards the IS, immediately after an intense and prolonged actin reorganization at the IS [14] (Suppl. Video 6). In contrast, in the P5 PKC $\delta$ -interfered clone, after a weak cortical actin reorganization at the IS, Cherry-paxillin in punctate structures remained non-polarized together with CFP-CD63 $^+$  MVB (Suppl. Video 6). We next studied whether paxillin could be phosphorylated by PKC $\delta$ . When we challenged C3 control clone with SEE-pulsed Raji cells, immunofluorescence analysis showed that paxillin, colocalizing with MTOC (Figure 7a and not shown) as previously described [44], was phosphorylated in T538 (Figure 7a). To analyse phosphorylation of paxillin, we carried out image quantitation analysis and found that the pT538-paxillin MFI signal induced upon IS formation was significantly higher in the C3 control clone than in the P5 PKC $\delta$ -interfered clone (Figure 7b). Since Raji cells express

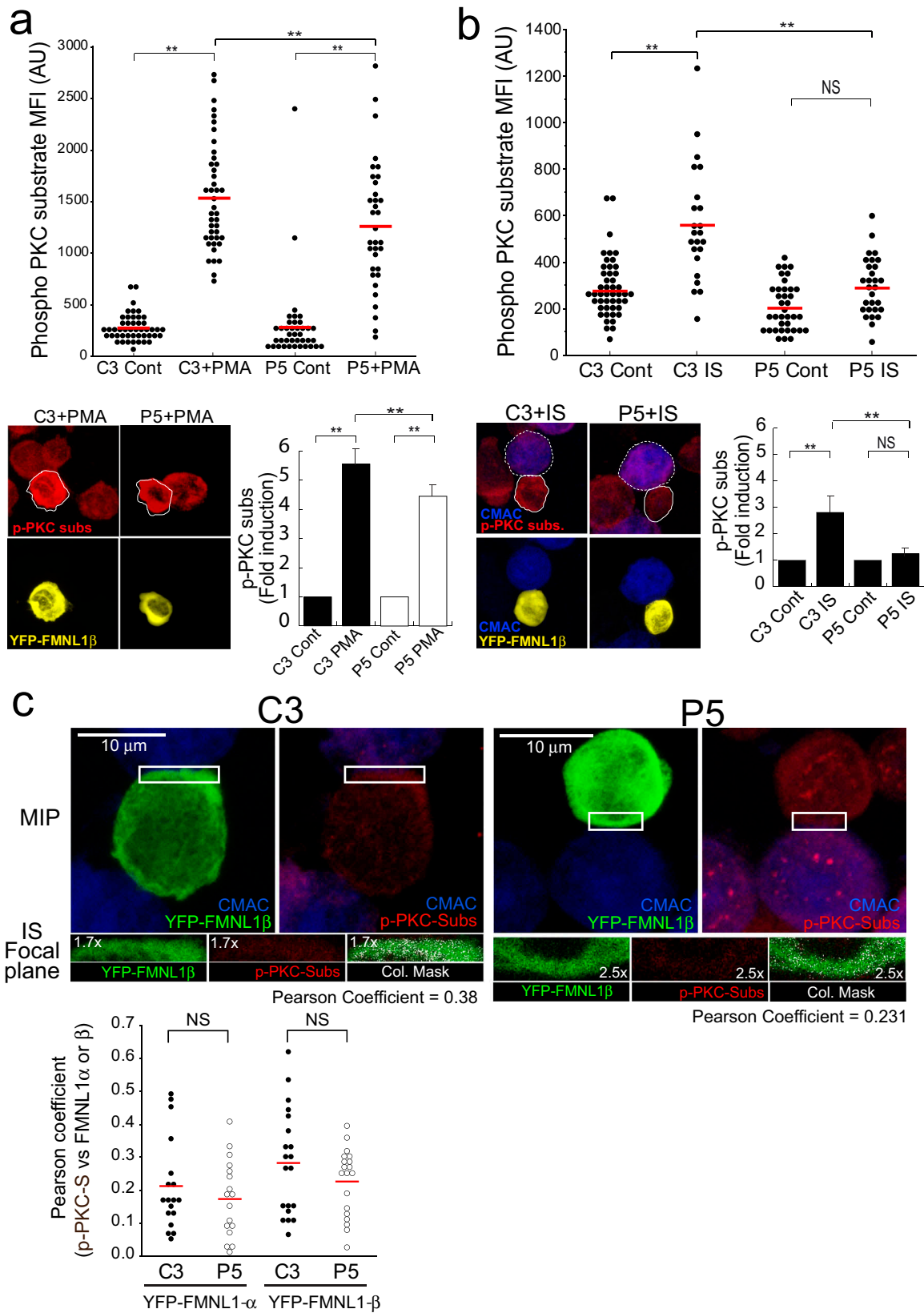


**Figure 6.** PKC $\delta$  induces FMNL1 $\beta$  phosphorylation.

C3 control and P5 PKC $\delta$ -interfered clones were transfected with an FMNL1-interfering, HA-YFP-FMNL1 $\beta$ -expressing vector (shFMNL1-HA-YFP-FMNL1 $\beta$ ). Subsequently, the transfected clones were either untreated (Cont), or stimulated with PMA (30 min), or challenged with CMAC-labelled SEE-pulsed Raji cells for 1 h, fixed, stained with anti-Phospho-(Ser) PKC substrate AF647 (magenta) and imaged by confocal fluorescence microscopy. Yellow channel fluorescence identifies the HA-YFP-FMNL1 $\beta$ -expressing cells. (Panel A), upper plot, Phospho-(Ser) PKC substrate

very high levels of paxillin (not shown), WB analysis of synaptic conjugates would not allow distinguishing Raji-derived paxillin from Jurkat clones-derived paxillin. Thus, to quantitate the relative, T538 paxillin phosphorylation by WB we stimulated control and PKC $\delta$ -interfered Jurkat clones with PMA or plastic-bound anti-TCR. An increase in pT538-paxillin signal was observed after stimulation of C3 control clone with PMA or anti-TCR (Figure 7c-d), which was partially associated with a mobility shift of paxillin. However, the normalized induction of phosphorylation in T538 paxillin by anti-TCR stimulation in the P5 PKC $\delta$ -interfered clone was significantly lower than in the C3 control clone (Figure 7d). Furthermore, GFP-PKC $\delta$  expression in P5 PKC $\delta$ -interfered clone stimulated with anti-TCR for 1 h raised T538 paxillin phosphorylation to the levels found in C3 control clone expressing GFP-PKC $\delta$  (Suppl. Fig. S11). Together these data indicate that PKC $\delta$  regulates phosphorylation and hence probably paxillin subcellular location and function during IS formation.

## Discussion

We have identified here for the first time a positive regulatory role of PKC $\delta$  acting on both FMNL1 $\beta$  and paxillin-controlled actin regulatory pathways that govern MTOC/MVB polarization to the IS in Th lymphocytes. FMNL1 $\beta$  and paxillin, most probably, coordinately control F-actin reorganization at the IS and around the MTOC, respectively, and may collaborate in MTOC polarization and subsequent exosome secretory traffic [14]. PKC $\delta$  is known to regulate polarized secretion in T lymphocytes [14,37,45], and directional migration [46,47], but no studies regarding the molecular bases controlling the PKC $\delta$  effect on polarized traffic have been reported to date. The spatial and temporal control

of F-actin polymerization is fundamental for many cellular processes including cell migration, division, vesicle trafficking, and response to agonists. In this context, T and B lymphocytes are the only cells in which agonists, namely antigens, by binding to their TCR and BCR at the IS, induce polarized MVB traffic [48] and exosome secretion [13,15,17,49]. This inducible polarized secretory traffic is controlled by actin cytoskeleton reorganization [5,14]. In this paper we have dissected some mechanisms by which two distinct networks of F-actin (cortical F-actin at the IS and centrosomal area F-actin) are reorganized and their contribution to the processes of MTOC and MVB polarization upon TCR activation at the IS.

The understanding of the diverse molecular mechanisms controlling the distinct F-actin networks is an important and general biological issue [50,51]. However, several contradictory results exist regarding the relative contribution of the different F-actin-regulatory pathways and the distinct F-actin networks to cell polarity in general [52,53], and to MTOC polarization and subsequent secretion in T lymphocytes in particular [5,7,23]. Thus, while some results suggest (but do not formally demonstrate) that the cortical actin reorganization at the IS is necessary and sufficient for MTOC/lytic granules and cytokine-containing granules polarization [5,7,22], several other evidences show that the two major F-actin-regulatory pathways (Arp2/3 acting on cortical F-actin network and FMNL1 on non-cortical F-actin network) can independently act in the regulation of MTOC polarization [23]. In this context, it has been shown that MTOC is a F-actin organizing centre [27] and centrosomal F-actin depletion appears to be crucial to allow MTOC polarization towards the IS in B lymphocytes stimulated with BCR-ligand-coated beads [28]. In the same B lymphocyte model, F-actin

MFI in the indicated (white line) cell ROI was calculated as described in Materials and Methods for C3 control and P5 clones expressing HA-YFP-FMNL1 $\beta$  either non-stimulated (Cont) or PMA-stimulated. The red line indicates the average Phospho-(Ser) PKC substrate MFI for each group. In the lower panel, left side, representative AIPs of the indicated channels of the transfected clones, stimulated with PMA, are shown. In the right side, quantification of Phospho-(Ser) PKC substrate MFI in C3 control and P5 clones expressing HA-YFP-FMNL1 $\beta$ , either non-stimulated (Cont) or PMA-stimulated, represented as fold induction of Phospho-(Ser) PKC substrate MFI (mean $\pm$ SD), summarizing the results obtained in several ( $n = 4$ ) experiments. Panel B, upper diagram, calculation of the Phospho-(Ser) PKC substrate MFI in the specified (continuous white line) cell ROI was calculated as indicated in Materials and Methods, for C3 control and P5 PKC $\delta$ -interfered clones expressing HA-YFP-FMNL1 $\beta$  either non-stimulated (Cont) or IS-stimulated. The red line indicates the average Phospho-(Ser) PKC substrate MFI for each group. In the lower left panel, representative AIPs of the indicated channels of the IS-stimulated transfected clones (Raji cells are labelled with a white discontinuous line) are shown. In the right side, quantification of Phospho-(Ser) PKC substrate MFI in C3 control and P5 PKC $\delta$ -interfered clones expressing HA-YFP-FMNL1 $\beta$ , either non-stimulated (Cont) or IS-stimulated, represented as fold induction of Phospho-(Ser) PKC substrate MFI (mean $\pm$ SD), and summarizing the results obtained in several ( $n = 5$ ) experiments. NS, not significant; \*\*,  $p \leq 0.05$ . (Panel C) IS conjugates made by C3 control and P5 PKC $\delta$ -interfered clones expressing HA-YFP-FMNL1 $\beta$  were imaged by confocal microscopy to analyse the colocalization of HA-YFP-FMNL1 $\beta$  and Phospho-(Ser) PKC substrate signals, as indicated in Materials and Methods. In the upper row, MIPs of the indicated channels are shown. The white rectangles enclose the IS ROIs that were used for colocalization analyses in the focal planes indicated in the lower row. Colocalization pixels are shown in white colour on the colocalizations masks, as well as the corresponding Pearson's coefficients. The lower plot shows the Pearson's coefficients corresponding to several analyses similar to the one shown in the upper row, for synapses made by C3 and P5 clones expressing HA-YFP-FMNL1 $\beta$  or HA-YFP-FMNL1 $\alpha$ . The red line indicates the average Pearson's coefficient for each cell group. NS, not significant.



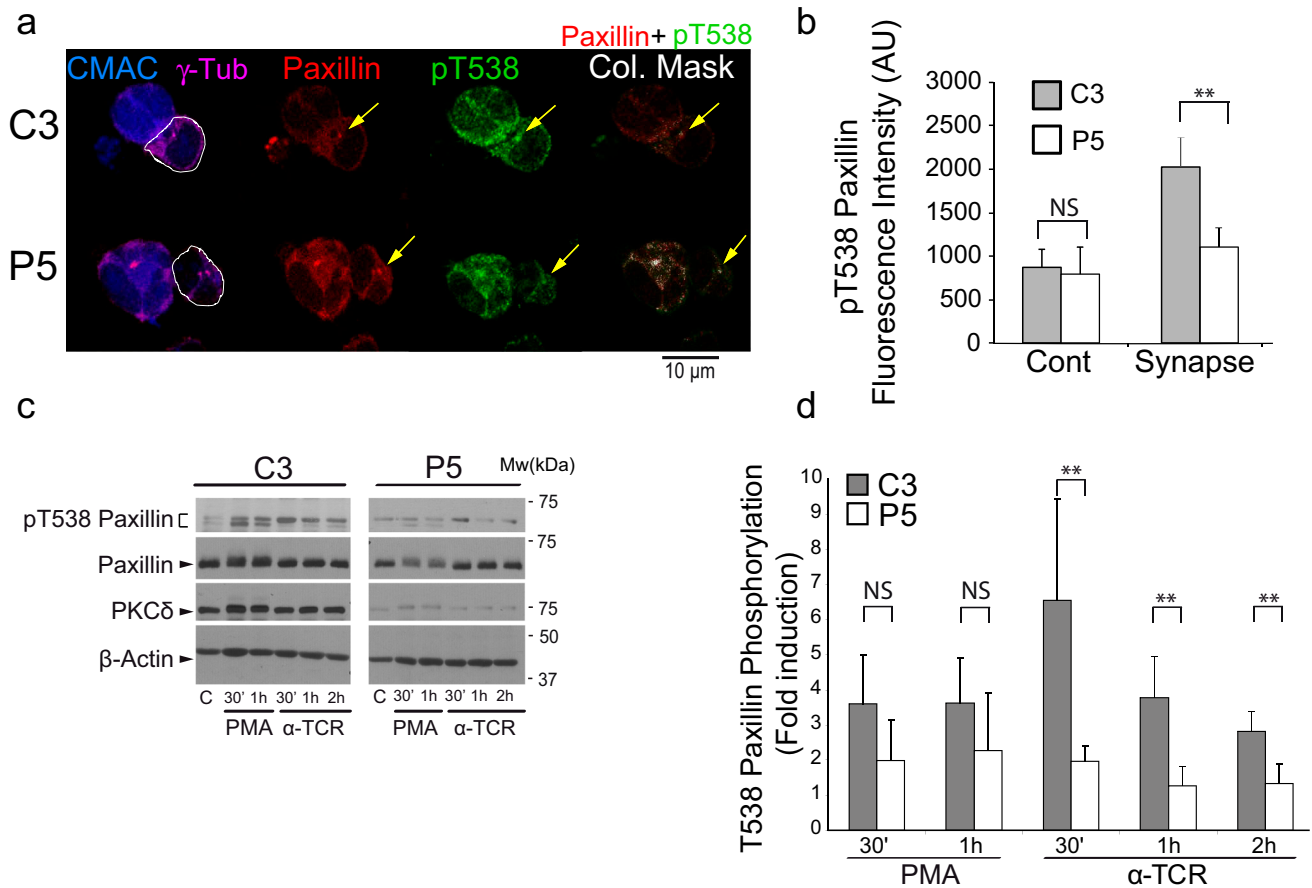


**Figure 7.** PKC $\delta$  regulates the phosphorylation of paxillin at T538.

(Panel A) C3 control and P5 PKC $\delta$ -interfered Jurkat clones were challenged with CMAC-labelled, SEE-pulsed Raji cells for 1 h, fixed, immunolabelled with anti- $\gamma$ -tubulin, anti-paxillin and anti-phospho-T538 paxillin and imaged by confocal microscopy. White lines enclose Jurkat cells. In the right panels, colocalization masks of merged, paxillin and phospho-T538 paxillin channels, are represented in white. The yellow arrows indicate accumulations of paxillin and phospho-T538 paxillin. CMAC labelling of Raji cells in blue,  $\gamma$ -tubulin (MTOC) in magenta, paxillin in red and phospho-T538 paxillin in green. (Panel B) C3 control and P5 PKC $\delta$ -interfered Jurkat clones were either untreated (Cont) or challenge with SEE-pulsed Raji cells (synapse) and immunolabelled as in A. Phospho-T538 paxillin signals were internally normalized to paxillin signals as described in Materials and Methods. (Panel C) C3 control and P5 PKC $\delta$ -interfered Jurkat clones untreated (c), or stimulated with either PMA or plastic-bound anti-TCR, were lysed at the indicated times. Cell lysates were analysed by WB with antibodies against phospho-T538-paxillin, paxillin, PKC $\delta$  and  $\beta$ -actin. (Panel D) Fold induction of paxillin T538 phosphorylation, normalized to paxillin levels, was evaluated by WB quantification of several experiments similar to that described in panel C. Data are means plus SD ( $n = 3$ ). NS, not significant; \*\*,  $p \leq 0.05$ .

depletion around the MTOC, F-actin reorganization at the IS, and MTOC polarization depend on proteasome activity [29]. These data do not allow inferring either the sufficiency or the relative contribution of each F-actin network (cortical and centrosomal) to MTOC polarization. In addition, the results of this B lymphocyte model cannot be directly extrapolated to T lymphocytes forming cell-to-cell conjugates as used here.

The above-mentioned results on B lymphocytes, together with our previous observation regarding the effect of PKC $\delta$  on cortical F-actin on the IS, prompted us to study the involvement of centrosomal area F-actin in MTOC polarization in cell-to-cell synapses made by T lymphocytes and its potential regulation by

PKC $\delta$ . We found a statistically significant negative correlation between MTOC polarization and centrosomal area F-actin (Figure 2b, please compare with Figure 5g from ref. [28]), and significant differences in centrosomal area F-actin among control and PKC $\delta$ -interfered clones (Figure 2c). The differences observed between the values of centrosomal area F-actin of control (0.93, C3; 0.99, C9) vs PKC $\delta$ -interfered clones (1.18, P5; 1.37, P6) (Figure 2c) were similar to those caused by proteasome inhibition in B lymphocytes (1.00 in control vs 1.25 in proteasome inhibitor-treated cells), that inhibited MTOC polarization [29]. Thus, it is conceivable that the centrosomal area F-actin changes we observed, alone or in combination with the alterations in cortical F-actin at the IS, may in

part underlie the deficiency in MTOC polarization in PKC $\delta$ -interfered clones (Figure 1b). The diameter determining the centrosome volume we have used (2  $\mu$ m) to measure centrosomal area F-actin includes the wide range of centrosome radius from prophase to metaphase (400–2000 nm) [54]. Thus, this volume centred at the MTOC can include all the potential oscillations in centrosome radius, which indeed were noticeable in some of our results when a pericentriolar marker (DsRed2 Centrin) was utilised (Figure 2d, lower panels). Although some authors have employed the same ROI size to measure centrosomal F-actin changes in polarizing lymphocytes [28], it cannot be excluded that other organelles reorganizing F-actin or tubulin cytoskeleton may be included in this area, such as the Golgi [30] or endosomes/MVB [55,56]. Among these organelles, we can rule out the contribution of F-actin at the Golgi to the observed MTOC polarization, since re-expression of FMNL1 $\gamma$ , which is the only FMNL1 isoform capable to regulate F-actin reorganization at the Golgi [30], was unable to rescue both centrosomal area F-actin and MTOC polarization to control levels (Suppl. Figs. S7 and S8). Regarding the presence of MVB in the centrosomal area, our results show that MVB are included in the 2  $\mu$ m MTOC-centred area (Figure 1, Suppl. Video 1 and Suppl. Fig. S1), and thus we cannot exclude the contribution of MVB to F-actin reorganization at the centrosomal area during centrosome reorientation. Since MVB and MTOC centre of masses are coincident and both organelles polarize (or not) together to the IS (Suppl. Fig. S1), the molecular mechanisms controlling these processes are, most probably, common for both simultaneously polarizing organelles. At this stage, we can only speculate about the necessity of the two F-actin reorganization processes or the sufficiency of one of these for MTOC polarization. In this context, FMNL1-interfered cells re-expressing FMNL1 $\beta$  exhibited high centrosomal area F-actin, polarized MTOC, and a significant F-actin depleted area at the central IS (Figure 5, Suppl. Fig. S9). This suggests that, when only the FMNL1 $\beta$  isoform is present, centrosomal area F-actin disorganization is not necessary, and F-actin reorganization at the IS is sufficient, for MTOC polarization. In addition, the fact that neither FMNL1 $\alpha$  nor FMNL1 $\gamma$  alone were capable to rescue both MTOC polarization (Suppl. Fig. S7) and centrosomal area F-actin (Suppl. Fig. S8) to control levels opens the possibility that any combination of FMNL1 $\beta$  with FMNL1 $\alpha$  or FMNL1 $\gamma$ , or the three isoforms acting together, may collaborate on centrosomal area F-actin reorganization.

Regarding the contribution of the FMNL1 isoforms present in T lymphocytes ( $\alpha$ ,  $\beta$  and  $\gamma$ ) [30] to the observed phenotype, and their potential role in PKC $\delta$ -dependent phosphorylation, it must be stressed that the anti-FMNL1 antibodies used for WB (C-5) and IP (clone A-4) recognized all these isoforms. In addition, the FMNL1-interfering vector transiently inhibiting the expression of all FMNL1 isoforms in Jurkat cells [30] decreased MTOC polarization to the levels observed in PKC $\delta$ -interfered clones (Figure 5a-b). Thus, at this stage we cannot ascribe the observed effect of PKC $\delta$  on FMNL1 to the phosphorylation of one or several FMNL1 isoforms. Experiments with FMNL1 suppression, FMNL1 isoform-specific re-expression vectors [30] were performed to analyse the phosphorylation of the different FMNL1 isoforms and their specific role in MTOC polarization, as well as their subcellular localization. FMNL1 $\beta$ , but not FMNL1 $\alpha$  or FMNL1 $\gamma$ , re-expression in YFP<sup>+</sup> FMNL1-interfered cells restored MTOC polarization to that of control, YFP<sup>-</sup> cells (Fig. 5A and Suppl. Fig. S7). In addition, we observed PMA- or IS formation-induced specific phosphorylation of FMNL1 $\beta$ , but not of FMNL1 $\alpha$ , FMNL1 $\gamma$  or a C-terminal deletion mutant FMNL1 (FMNL1- $\Delta$ FH2) (Figure 6b, Suppl. Fig. S10). The decrease in Phospho-(Ser) PKC substrate MFI signal induced by PMA stimulation occurring in HA-YFP-FMNL1 $\alpha$ , HA-YFP-FMNL1 $\gamma$  and HA-YFP-FMNL1 $\Delta$ FH2 (Suppl. Fig. S10B), but not in HA-YFP-FMNL1 $\beta$ -expressing cells (Suppl. Fig. S10A), when compared with non-transfected cells (Suppl. Fig. S10, compare panel A with panel B) is, most probably, caused by the interference in endogenous FMNL1 $\beta$  expression. FMNL1 $\beta$  possesses, but FMNL1 $\alpha$ , FMNL1 $\gamma$  and FMNL1- $\Delta$ FH2 lack, a potential PKC phosphorylation site (S1086 in FMNL1 $\beta$ ) in the DAD auto-inhibitory domain with high homology to that of FMNL2 (S1072) [41,42] (Suppl. Fig. S6). The three FMNL1 isoforms share identical sequence from amino acid residue 1–1070, and diverge in the C-terminal region (Suppl. Fig. S6), which includes the DAD auto-inhibitory domain. PMA- and IS formation-induced FMNL1 $\beta$  phosphorylation, as well as IS formation-induced MTOC polarization, were decreased in P5 PKC $\delta$ -interfered clone (Figure 6). Taken together, these results support that IS-induced, PKC $\delta$ -dependent phosphorylation in FMNL1 $\beta$  C-terminal region containing the auto-inhibitory domain (possibly at S1086) activates FMNL1 $\beta$  and mediates MTOC polarization. Further experiments re-expressing a mutated FMNL1 $\beta$  non-phosphorylatable at S1086 (equivalent to FMNL2-S1072A described in [41]), are necessary to fully confirm this hypothesis and to study its role in MTOC polarization. In addition, it will be interesting to analyse whether a non-phosphorylatable FMNL1 $\beta$  mutant can rescue the relative

F-actin-low cIS area as occurs with WT FMNL1 $\beta$  (Suppl. Fig. S9). FMNL1 or PKC $\delta$  interference inhibited MTOC polarization to similar extent (Figure 5b), suggesting that PKC $\delta$  and FMNL1 participate in the same F-actin regulatory pathway controlling MTOC polarization. In addition, FMNL1 interference in a PKC $\delta$ -interfered clone did not further decrease MTOC polarization (Figure 5b), which is compatible with PKC $\delta$  and FMNL1 participating in the same F-actin regulatory pathway. Additional experiments will be necessary to formally address this point.

DAG and its negative regulator DGK $\alpha$  play essential roles in TCR-induced MVB and late endosomes polarized traffic and lytic granule secretion [15,16,57–59], but the molecular mechanisms involved remained largely unknown. We have previously established that PKC $\delta$  is necessary for MTOC/MVB polarization [14]. In addition, we have shown that TCR activation at the IS induces PKC $\delta$  activation, which appears to be mediated by DAG-induced, PKC $\delta$  recruitment to MVB endomembranes [14]. We show here that upon IS formation activated PKC $\delta$ , directly or indirectly, induces FMNL1 $\beta$  phosphorylation at its C-terminal, autoregulatory region, possibly at S1086, although this has not been demonstrated yet. This may release FMNL1 $\beta$  from its C-terminal autoinhibitory domain, rendering FMNL1 $\beta$  capable of reorganizing F-actin at the IS. In addition, FMNL1 colocalizes with F-actin at the IS but not with centrosomal area F-actin (Figure 3), suggesting that FMNL1 mainly governs synaptic F-actin. Our results showing that PKC $\delta$  interference does not affect FMNL1 location in F-actin reorganization areas (Figure 3) capable to regulate MTOC polarization [5,23,27,28,60] is consistent with the idea that posttranslational modifications of FMNL1 such as phosphorylation, but not changes in FMNL1 subcellular location, may underlie PKC $\delta$ -mediated control of FMNL1 function.

Regarding the potential mechanisms involved in centrosomal area F-actin disassembly and MTOC polarization, PKC $\delta$  and paxillin colocalize in polarized T lymphocytes at or nearby the MTOC [14,25,26,44,46,61], the location where we observed T538-phosphorylated paxillin (Figure 7a). Paxillin and FMNL1 $\beta$  may thus coordinately regulate F-actin reorganization around the MTOC and at the IS, respectively. This possibility is supported by the fact that PKC $\delta$  interference decreases paxillin phosphorylation and enhances F-actin around the MTOC that, most probably, subsequently inhibits MTOC/MVB polarization (Figure 1 and Suppl. Videos 2, 4 and 5) and exosome secretion at the IS [14] and AICD (Suppl. Video 4). PKC $\delta$  phosphorylates paxillin at T538 in vitro and in vivo, leading to F-actin

depolymerization during integrin-mediated adhesion of a B cell line [43]. Furthermore, paxillin is constitutively associated with the MTOC in T lymphocytes [26,44] and, upon target cell binding, with the peripheral SMAC (pSMAC) at the IS in CTLs [25]. Moreover, interfering with paxillin impedes MTOC polarization [25]. In CTLs, paxillin phosphorylation regulates the MTOC polarization to the IS [25]. However, we were unable to detect any paxillin accumulation at the IS when we observed the burst of F-actin at the IS (Suppl. Video 6, Figure 7). Thus, in our Th model, PKC $\delta$ -dependent paxillin phosphorylation may govern F-actin reorganizations at locations different from the IS, such as around the MTOC, that may also contribute to the diminished MTOC polarization observed in PKC $\delta$ -interfered clones. This hypothesis is supported by the decrease of paxillin phosphorylation in PKC $\delta$ -interfered clones (Figure 7) and its reversal by GFP-PKC $\delta$  (Suppl. Fig. S11), which also causes the recovery of the spatial and temporal reorganization of F-actin at the IS and MVB polarization to the IS [14]. This PKC $\delta$ -dependent, paxillin-regulated mechanism for centrosomal area F-actin reorganization appears to co-exist in T lymphocytes with the PKC $\delta$ -dependent, FMNL1 $\beta$ -regulated mechanism for cortical F-actin reorganization. More research is necessary (i.e. experiments involving a phospho-deficient mutant of paxillin at 538 residue) to establish the relative contribution of this mechanism to the polarization processes.

With respect to the biological significance of these finely tuned and coordinated actin cytoskeleton regulatory mechanisms involved in MTOC polarization, it is remarkable that centrosomal area F-actin reorganization is triggered by antigen-receptor stimulation, which is a common event occurring both in B [28] and T lymphocytes (this paper) forming IS. In BCR-stimulated B lymphocytes, apart of F-actin reorganization at the IS [48], centrosomal F-actin-reorganization controls polarized and local secretion of lysosomes at the synaptic cleft that is involved in antigen extraction from APC, a crucial event involved in antigen processing and the acquisition of B cell-effector functions [29,48,62]. In T lymphocytes, a comparable centrosomal area F-actin reorganization regulates MTOC and MVB polarization (this paper) that eventually leads to secretory granule secretion (including exosomes) [14]. Remarkably, T and B lymphocytes share the ability to form IS with APC, a crucial event involved in the immune response upon antigen challenge via TCR or BCR stimulation [48,63], and this induces exosome secretion [17,64]. The IS is a highly dynamic and plastic signalling platform induced by antigen receptors stimulation and triggers exquisite mechanisms leading to optimal polarized and

focused secretion at the synaptic cleft, to avoid the stimulation (or death) of bystander cells [1,9,35,48,65], or the non-specific extraction of antigens from APC [29,62]. The existence in T lymphocytes of at least two PKC $\delta$ -controlled, coordinated regulatory mechanisms acting on two distinct F-actin networks, both controlling MTOC polarization and secretion, may establish subtle regulatory checkpoints to finely control IS-triggered polarized secretion, as previously suggested [23]. Polarized secretion guarantees the antigen specificity of the final response in many cell lineages of the immune system, including innate NK cells [66,67], CTL [5,38], B lymphocytes [29,62], primary CD4 + T cells [68] and Jurkat cells [38]. The association of the absence of PKC $\delta$  with the generation of B and T lymphoproliferative disorders both in human and mice [69,70], and the participation of PKC $\delta$  in the homeostasis of blood progenitors [71], support the important role of PKC $\delta$  in maintaining cell homeostasis. Further approaches are needed to extend our results regarding the contribution of PKC $\delta$ -dependent centrosomal area F-actin to polarized and focused secretion in directional and invasive cell migration, both of lymphoid and non-lymphoid cells. These approaches would clarify whether centrosomal area F-actin reorganization occurs only during IS formation or also participates in other biologically relevant cellular polarization processes.

## Acknowledgments

We are indebted and acknowledge Dr D.D. Billadeau (Mayo Clinic, USA) for generous sharing of shFMNL1 and FMNL1 isoform rescue constructions. We acknowledge the excellent technical support from A. Sánchez and A. Garrido. We acknowledge Dr A. Anel (Universidad de Zaragoza, Spain) for suggestions and critical reading of this manuscript and Dr M.A. Alonso (CBM, CSIC) for reagents and scientific advice. Thanks to D. Morales (SIDI-UAM) and S. Gutiérrez (CNB, CSIC) for their superb expertise with confocal microscopy. This work was supported by grants from the Spanish Ministerio de Economía y Competitividad (MINECO), Plan Nacional de Investigación Científica (SAF2016-77561-R to M.I., which was in part granted with FEDER-EC funding).

## Disclosure statement

The authors report no conflict of interest.

## Funding

This work was supported by the Ministerio de Ciencia, Innovación y Universidades [SAF2016-77561-R]; Ministerio de Economía y Competitividad [SAF2016-77561-R].

## Author Contributions Statement

V.C. and M.I. conceived and designed all the experiments. A. B., R.I., M.V., S.M., G.H., S.H. and V.C. did most of the experiments, analysed data, and contributed to the writing of the manuscript. A.B., R.I. contributed to the MTOC/MVB polarization experiments and IS image analyses. A. B. performed the FMNL1 immunoprecipitation experiments. L.M. M.V. and S. M. contributed to the FMNL1 phosphorylation studies and image analyses, and M.V., S.M., J.B. and G.H. contributed to time-lapse studies and image analyses of area F-actin. A.S. performed the WB analysis and also contributed to paxillin phosphorylation experiments. M. I. conceptualized and coordinated the research, directed the study, analysed data, and wrote the manuscript. All the authors contributed to the planning and designing of the experiments and to helpful discussions.

## ORCID

Jorge Bernardino De La Serna  <http://orcid.org/0000-0002-1396-3338>

Víctor Calvo  <http://orcid.org/0000-0002-5913-7058>

Manuel Izquierdo  <http://orcid.org/0000-0002-7701-1002>

## References

- [1] de la Roche M, Asano Y, Griffiths GM. Origins of the cytolytic synapse. *Nat Rev Immunol*. 2016;16(7):421–432.
- [2] Huse M. Microtubule-organizing center polarity and the immunological synapse: protein kinase C and beyond. *Front Immunol*. 2012;3:235.
- [3] Billadeau DD, Nolz JC, Gomez TS. Regulation of T-cell activation by the cytoskeleton. *Nat Rev Immunol*. 2007;7(2):131–143.
- [4] Griffiths GM, Tsun A, Stinchcombe JC. The immunological synapse: a focal point for endocytosis and exocytosis. *J Cell Biol*. 2010;189(3):399–406.
- [5] Ritter AT, Asano Y, Stinchcombe JC, et al. Actin depletion initiates events leading to granule secretion at the immunological synapse. *Immunity*. 2015;42(5):864–876.
- [6] Ritter AT, Kapnick SM, Murugesan S, et al. Cortical actin recovery at the immunological synapse leads to termination of lytic granule secretion in cytotoxic T lymphocytes. *Proc Natl Acad Sci U S A*. 2017;114:E6585–E6594.
- [7] Chemin K, Bohineust A, Dogniaux S, et al. Cytokine secretion by CD4+ T cells at the immunological synapse requires Cdc42-dependent local actin remodeling but not microtubule organizing center polarity. *J Immunol*. 2012;189(5):2159–2168.
- [8] Fooksman DR, Vardhana S, Vasiliver-Shamis G, et al. Functional anatomy of T cell activation and synapse formation. *Annu Rev Immunol*. 2010;28:79–105.
- [9] Xie J, Tato CM, Davis MM. How the immune system talks to itself: the varied role of synapses. *Immunol Rev*. 2013;251(1):65–79.
- [10] Huse M, Quann EJ, Davis MM. Shouts, whispers and the kiss of death: directional secretion in T cells. *Nat Immunol*. 2008;9(10):1105–1111.



- [11] Peters PJ, Borst J, Oorschot V, et al. Cytotoxic T lymphocyte granules are secretory lysosomes, containing both perforin and granzymes. *J Exp Med*. 1991;173(5):1099–1109.
- [12] Peters PJ, Geuze HJ, Van der Donk HA, et al. Molecules relevant for T cell-target cell interaction are present in cytolytic granules of human T lymphocytes. *Eur J Immunol*. 1989;19(8):1469–1475.
- [13] de Saint Basile G, Menasche G, Fischer A. Molecular mechanisms of biogenesis and exocytosis of cytotoxic granules. *Nat Rev Immunol*. 2010;10(8):568–579.
- [14] Herranz G, Aguilera P, Davila S, et al. Protein kinase c delta regulates the depletion of actin at the immunological synapse required for polarized exosome secretion by T cells. *Front Immunol*. 2019;10:851.
- [15] Alonso R, Mazzeo C, Rodriguez MC, et al. Diacylglycerol kinase alpha regulates the formation and polarisation of mature multivesicular bodies involved in the secretion of fas ligand-containing exosomes in T lymphocytes. *Cell Death Differ*. 2011;18(7):1161–1173.
- [16] Alonso R, Rodriguez MC, Pindado J, et al. Diacylglycerol kinase alpha regulates the secretion of lethal exosomes bearing Fas ligand during activation-induced cell death of T lymphocytes. *J Biol Chem*. 2005;280(31):28439–28450.
- [17] Mazzeo C, Calvo V, Alonso R, et al. Protein kinase D1/2 is involved in the maturation of multivesicular bodies and secretion of exosomes in T and B lymphocytes. *Cell Death Differ*. 2016;23(1):99–109.
- [18] Martinez-Lorenzo MJ, Anel A, Gamen S, et al. Activated human T cells release bioactive Fas ligand and APO2 ligand in microvesicles. *J Immunol*. 1999;163(3):1274–1281.
- [19] Nagata S. Apoptosis by death factor. *Cell*. 1997;88(3):355–365.
- [20] Kühn S, Geyer M. Formins as effector proteins of Rho GTPases. *Small GTPases*. 2014;5:e29513.
- [21] Kumari S, Curado S, Mayya V, et al. T cell antigen receptor activation and actin cytoskeleton remodeling. *Biochim Biophys Acta*. 2014;1838(2). DOI:10.1016/j.bbmem.2013.05.004
- [22] Sanchez E, Liu X, Huse M. Actin clearance promotes polarized dynein accumulation at the immunological synapse. *PloS One*. 2019;14(7):e0210377.
- [23] Gomez TS, Kumar K, Medeiros RB, et al. Formins regulate the actin-related protein 2/3 complex-independent polarization of the centrosome to the immunological synapse. *Immunity*. 2007;26(2):177–190.
- [24] Romanova LY, Mushinski JF. Central role of paxillin phosphorylation in regulation of LFA-1 integrins activity and lymphocyte migration. *Cell Adh Migr*. 2011;5(6):457–462.
- [25] Robertson LK, Ostergaard HL. Paxillin associates with the microtubule cytoskeleton and the immunological synapse of CTL through its leucine-aspartic acid domains and contributes to microtubule organizing center reorientation. *J Immunol*. 2011;187(11):5824–5833.
- [26] Robertson LK, Mireau LR, Ostergaard HL. A role for phosphatidylinositol 3-kinase in TCR-stimulated ERK activation leading to paxillin phosphorylation and CTL degranulation. *J Immunol*. 2005;175(12):8138–8145.
- [27] Farina F, Gaillard J, Guerin C, et al. The centrosome is an actin-organizing centre. *Nat Cell Biol*. 2016;18(1):65–75.
- [28] Obino D, Farina F, Malbec O, et al. Actin nucleation at the centrosome controls lymphocyte polarity. *Nat Commun*. 2016;7:10969.
- [29] Ibanez-Vega J, Del Valle Batalla F, Saez JJ, et al. Proteasome dependent actin remodeling facilitates antigen extraction at the immune synapse of B cells. *Front Immunol*. 2019;10:225.
- [30] Colon-Franco JM, Gomez TS, Billadeau DD. Dynamic remodeling of the actin cytoskeleton by FMNL1gamma is required for structural maintenance of the golgi complex. *J Cell Sci*. 2011;124(Pt 18):3118–3126.
- [31] Montoya MC, Sancho D, Bonello G, et al. Role of ICAM-3 in the initial interaction of T lymphocytes and APCs. *Nat Immunol*. 2002;3(2):159–168.
- [32] Bello-Gamboa A, Izquierdo JM, Velasco M, et al. Imaging the human immunological synapse. *Journal of Visualized Experiments*. In Press (2019); 154. DOI: 10.3791/60312
- [33] Abrahamsen G, Sundvold-Gjerstad V, Habtamu M, et al. Polarity of CD4+ T cells towards the antigen presenting cell is regulated by the Lck adapter TSAd. *Sci Rep*. 2018;8(1):13319.
- [34] Jambirina E, Alonso R, Alcalde M, et al. Calcium influx through receptor-operated channel induces mitochondria-triggered paraptotic cell death. *J Biol Chem*. 2003;278(16):14134–14145.
- [35] Calvo V, Izquierdo M. Imaging polarized secretory traffic at the immune synapse in living T lymphocytes. *Front Immunol*. 2018;9:684.
- [36] Bertrand F, Muller S, Roh KH, et al. An initial and rapid step of lytic granule secretion precedes microtubule organizing center polarization at the cytotoxic T lymphocyte/target cell synapse. *Proc Natl Acad Sci U S A*. 2013;110(15):6073–6078.
- [37] Ma JS, Monu N, Shen DT, et al. Protein kinase Cdelta regulates antigen receptor-induced lytic granule polarization in mouse CD8+ CTL. *J Immunol*. 2007;178(12):7814–7821.
- [38] Nath S, Christian L, Tan SY, et al. Dynein separately partners with NDE1 and dynactin to orchestrate T cell focused secretion. *J Immunol*. 2016;197(6):2090–2101.
- [39] Yi J, Wu X, Chung AH, et al. Centrosome repositioning in T cells is biphasic and driven by microtubule end-on capture-shrinkage. *J Cell Biol*. 2013;202(5):779–792.
- [40] Lukinavicius G, Reymond L, D'Este E, et al. Fluorogenic probes for live-cell imaging of the cytoskeleton. *Nat Methods*. 2014;11(7):731–733.
- [41] Wang Y, Arjonen A, Pouwels J, et al. Formin-like 2 promotes  $\beta$ 1-integrin trafficking and invasive motility downstream of PKC $\alpha$ . *Dev Cell*. 2015;34(4):475–483.
- [42] Han Y, Eppinger E, Schuster IG, et al. Formin-like 1 (FMNL1) is regulated by N-terminal myristoylation and induces polarized membrane blebbing. *J Biol Chem*. 2009;284(48):33409–33417.
- [43] Romanova LY, Holmes G, Bahte SK, et al. Phosphorylation of paxillin at threonine 538 by PKCdelta regulates LFA1-mediated adhesion of lymphoid cells. *J Cell Sci*. 2010;123(Pt 9):1567–1577.
- [44] Herreros L, Rodriguez-Fernandez JL, Brown MC, et al. Paxillin localizes to the lymphocyte microtubule organizing center and associates with the

- microtubule cytoskeleton. *J Biol Chem.* **2000**;275(34):26436–26440.
- [45] Ma JS, Haydar TF, Radoja S. Protein kinase C delta localizes to secretory lysosomes in CD8+ CTL and directly mediates TCR signals leading to granule exocytosis-mediated cytotoxicity. *J Immunol.* **2008**;181(7):4716–4722.
- [46] Volkov Y, Long A, Kelleher D. Inside the crawling T cell: leukocyte function-associated antigen-1 cross-linking is associated with microtubule-directed translocation of protein kinase C isoenzymes beta(I) and delta. *J Immunol.* **1998**;161(12):6487–6495.
- [47] Wei SY, Lin TE, Wang WL, et al. Protein kinase C-delta and -beta coordinate flow-induced directionality and deformation of migratory human blood T-lymphocytes. *J Mol Cell Biol.* **2014**;6(6):458–472.
- [48] Yuseff MI, Lankar D, Lennon-Dumenil AM. Dynamics of membrane trafficking downstream of B and T cell receptor engagement: impact on immune synapses. *Traffic.* **2009**;10(6):629–636.
- [49] Thery C, Ostrowski M, Segura E. Membrane vesicles as conveyors of immune responses. *Nat Rev Immunol.* **2009**;9(8):581–593.
- [50] Suarez C, Kovar DR. Internetwork competition for monomers governs actin cytoskeleton organization. *Nat Rev Mol Cell Biol.* **2016**;17(12):799–810.
- [51] Skruber K, Read TA, Vitriol EA. Reconsidering an active role for G-actin in cytoskeletal regulation. *J Cell Sci.* **2018**;131(1). DOI:10.1242/jcs.203760
- [52] Chhabra ES, Higgs HN. The many faces of actin: matching assembly factors with cellular structures. *Nat Cell Biol.* **2007**;9(10):1110–1121.
- [53] Inagaki N, Katsuno H. Actin waves: origin of cell polarization and migration? *Trends Cell Biol.* **2017**;27(7):515–526.
- [54] Decker M, Jaensch S, Pozniakovsky A, et al. Limiting amounts of centrosome material set centrosome size in *C. elegans* embryos. *Curr Biol.* **2011**;21(15):1259–1267.
- [55] Calabia-Linares C, Robles-Valero J, de la Fuente H, et al. Endosomal clathrin drives actin accumulation at the immunological synapse. *J Cell Sci.* **2011**;124(Pt 5):820–830.
- [56] Ueda H, Morphew MK, McIntosh JR, et al. CD4+ T-cell synapses involve multiple distinct stages. *Proc Natl Acad Sci U S A.* **2011**;108(41):17099–17104.
- [57] Quann EJ, Merino E, Furuta T, et al. Localized diacylglycerol drives the polarization of the microtubule-organizing center in T cells. *Nat Immunol.* **2009**;10(6):627–635.
- [58] Rainero E, Caswell PT, Muller PA, et al. Diacylglycerol kinase alpha controls RCP-dependent integrin trafficking to promote invasive migration. *J Cell Biol.* **2012**;196(2):277–295.
- [59] Rainero E, Norman JC. Late endosomal and lysosomal trafficking during integrin-mediated cell migration and invasion: cell matrix receptors are trafficked through the late endosomal pathway in a way that dictates how cells migrate. *BioEssays.* **2013**;35(6):523–532.
- [60] Gomez TS, McCarney SD, Carrizosa E, et al. HS1 functions as an essential actin-regulatory adaptor protein at the immune synapse. *Immunity.* **2006**;24(6):741–752.
- [61] Fanning A, Volkov Y, Freeley M, et al. CD44 cross-linking induces protein kinase C-regulated migration of human T lymphocytes. *Int Immunol.* **2005**;17(4):449–458.
- [62] Saez JJ, Diaz J, Ibanez J, et al. The exocyst controls lysosome secretion and antigen extraction at the immune synapse of B cells. *J Cell Biol.* **2019**. DOI:10.1083/jcb.201811131
- [63] Harwood NE, Batista FD. Early events in B cell activation. *Annu Rev Immunol.* **2010**;28:185–210.
- [64] Alonso R, Mazzeo C, Merida I, et al. A new role of diacylglycerol kinase alpha on the secretion of lethal exosomes bearing Fas ligand during activation-induced cell death of T lymphocytes. *Biochimie.* **2007**;89(2):213–221.
- [65] Dustin ML, Choudhuri K. Signaling and Polarized communication across the T cell immunological synapse. *Annu Rev Cell Dev Biol.* **2016**;32:303–325.
- [66] Mentlik AN, Sanborn KB, Holzbaur EL, et al. Rapid lytic granule convergence to the MTOC in natural killer cells is dependent on dynein but not cytolytic commitment. *Mol Biol Cell.* **2010**;21(13):2241–2256.
- [67] Hsu H-T, Mace EM, Carisey AF, et al. NK cells converge lytic granules to promote cytotoxicity and prevent bystander killing. *J Cell Biol.* **2016**;215:875–889.
- [68] Ueda H, Zhou J, Xie J, et al. Distinct roles of cytoskeletal components in immunological synapse formation and directed secretion. *J Immunol.* **2015**;195(9):4117–4125.
- [69] Kuehn HS, Niemela JE, Rangel-Santos A, et al. Loss-of-function of the protein kinase C delta (PKCdelta) causes a B-cell lymphoproliferative syndrome in humans. *Blood.* **2013**;121(16):3117–3125.
- [70] Gorelik G, Sawalha AH, Patel D, et al. T cell PKCdelta kinase inactivation induces lupus-like autoimmunity in mice. *Clin Immunol.* **2015**;158(2):193–203.
- [71] Rao TN, Gupta MK, Softic S, et al. Attenuation of PKCdelta enhances metabolic activity and promotes expansion of blood progenitors. *Embo J.* **2018**;37(24). DOI:10.15252/embj.2018100409